Marine and Petroleum Geology 80 (2017) 538–562

Contents lists available at ScienceDirect

Marine and Petroleum Geology

journal homepage: www.elsevier.com/locate/marpetgeo

Research paper

Effects of oil cracking on fluorescence color, homogenization temperature and trapping pressure reconstruction of oil inclusions from deeply buried reservoirs in the northern Dongying Depression, Bohai Bay Basin, China

Hongwei Ping [a, b, *], Honghan Chen [a], Régis Thiéry [c], Simon C. George [b]

[a] Key Laboratory of Tectonics and Petroleum Resources, Ministry of Education, China University of Geosciences, Wuhan 430074, China
[b] Department of Earth and Planetary Sciences and Macquarie University Marine Research Centre, Macquarie University, North Ryde, Sydney, NSW 2109, Australia
[c] UMR 6524 'Magmas et Volcans', Universite Blaise Pascal, 5, Rue Kessler, F-63038 Clermont-Ferrand Cedex, France

ARTICLE INFO

Article history:
Received 8 July 2016
Received in revised form
21 December 2016
Accepted 26 December 2016
Available online 27 December 2016

Keywords:
Petroleum inclusion
Fluorescence spectroscopy
Homogenization temperature
Trapping pressure
Overpressure
Pyrobitumen
Oil cracking kinetics
Petroleum inclusion thermodynamics modeling

ABSTRACT

The effects of oil cracking on fluorescence color, homogenization temperature (T_{ho}) and trapping pressure (P_t) of oil inclusions from deeply buried reservoirs (DBRs) (3672–4359 m) in the northern Dongying Depression were determined based on fluorescence spectroscopy and homogenization temperatures of oil inclusions, kinetic modeling of crude oil cracking, and petroleum inclusion thermodynamics modeling.

The modeling results demonstrate that fluorescence color, T_{ho} and predicted P_t have strong relationships with the transformation rate via cracking of oil to gas (T_r), and the formation temperature (T_f) that the inclusions experienced. The fluorescence color is hardly influenced at all during the initial stages of oil cracking (T_r < 13%, T_f < 160 °C), but fluorescence color begins to shift toward shorter wavelengths (blue shift) during progressive oil cracking (T_r < 24%, T_f < 190 °C). With further oil cracking, the fluorescence color may either experience no change or continue its blue shift. Eventually the fluorescence color will disappear as the aromatic compounds are completely cracked. The T_{ho} increases at first (T_r < 24%, T_f < 190 °C), but then decreases or even becomes negative during major oil cracking. The reconstructed P_t values show a corresponding reverse trend.

Oil inclusions from DBRs and other shallow reservoirs in the Dongying Depression show an obvious blue shift in fluorescence color at a depth of approximate 4000 m (T_f = 160 °C) and generally contain solid bitumen below 4000 m, supporting the effect of oil cracking on fluorescence variation, consistent with the modeling result. The T_{ho} from DBRs in the Minfeng area increases with increasing burial depth (T_f < 190 °C), which is also consistent with the modeling results. However, the T_{ho} of oil inclusions with blue-white fluorescence from DBRs in the Shengtuo area did not show such a trend. Recent trapping, high trapping pressure and higher-maturity oil may have led to a low-degree of oil cracking, and thus less modification of T_{ho} in the Shengtuo area.

Oil cracking results in consistent volume ratios of pyrobitumen to oil inclusions (F_{vpy}) in the same fluid inclusion assemblage, and the F_{vpy} value increases with oil cracking level, which can be used to recognize if oil cracking has occurred in oil inclusions and what level of oil cracking they have experienced.

As the oil cracking model used in this study did not account for the role of pressure, it is more applicable for oil inclusions that were trapped under normally pressured conditions. Oil inclusions trapped under overpressured conditions will be less influenced by oil cracking.

1. Introduction

Oil inclusions are tiny droplets that are trapped within mineral grains as oil migrates. The composition, temperature and pressure

* Corresponding author. Key Laboratory of Tectonics and Petroleum Resources, Ministry of Education, China University of Geosciences, Wuhan 430074, China.
E-mail addresses: howping@qq.com (H. Ping), hhchen@cug.edu.cn (H. Chen), r.thiery@opgc.univ-bpclermont.fr (R. Thiéry), Simon.George@mq.edu.au (S.C. George).

http://dx.doi.org/10.1016/j.marpetgeo.2016.12.024
0264-8172/

of trapped oil inclusions have been used to decipher petroleum filling histories (Horsfield and McLimans, 1984; Karlsen et al., 1993; McLimans, 1987). Petroleum inclusion thermodynamics modeling, which integrates the homogenization temperature (T_{ho}), degree of bubble filling (F_{vo}) of an oil inclusion at room temperature (20 °C), and homogenization temperature of coeval aqueous fluid inclusion (T_{ha}), has become an effective method to reconstruct the evolution of pressure, temperature and composition (PTX) during petroleum charging and to trace the dynamic processes of paleo-oil and -gas migration and accumulation (Aplin et al., 1999; Bourdet et al., 2012; Ping et al., 2013; Thiéry et al., 2002). However, the accuracy of PTX reconstruction depends on both the petroleum inclusion thermodynamics modeling method itself, such as the choice of compositional model and thermodynamic parameters (Ping et al., 2011, 2013), and whether the input parameters (such as T_{ho}, F_{vo} and T_{ha}) for the modeling can precisely reflect the trapping conditions of the oil inclusions. Specifically, were the inclusions trapped in a homogenous phase, and did the volume and components of the fluid inclusions change after being trapped? (Roedder, 1984).

Oil cracking is an important mechanism for changing reservoired oil into light oil and natural gas in deep basins (Hao et al., 2008; Hu et al., 2010; Isaksen, 2004; Zhao et al., 2005). The process of oil cracking forms hydrogen-rich light hydrocarbon components and a pyrobitumen residue, which is poor in hydrogen and rich in carbon (Behar et al., 1992; Hill et al., 2003; Ungerer et al., 1988). Studies on synthetic hydrocarbon inclusions have shown that oil cracking not only occurs in natural oil accumulations but also in inclusions with thermal stress (Teinturier et al., 2003). Oil cracking changes the composition of oil inclusions, so the fluorescence color and microthermometry parameters (T_{ho} and F_{vo}) are expected to be affected. The variations of fluorescence color and fluorescence spectra of oil inclusions during artificial heating to 250–440 °C have been observed by several heating experiments (Dutkiewicz et al., 2003; Guilhaumou et al., 1990; Huang and Otten, 2001; Pironon and Pradier, 1992). Okubo (2005) discussed the influence of oil cracking on the T_{ho} of oil inclusions in quartz that was heated in an autoclave, and attributed the larger differences in the T_{ho} and T_{ha} values from the Shin-Kumoide SK-1D well to thermal cracking in the oil inclusions, and concluded that this effect can be observed around 120 °C. However, T_{ho} is jointly controlled by its trapping temperature (T_t), trapping pressure (P_t) and composition (Ping and Chen, 2011). During oil cracking, the composition, volume and internal pressure of oil inclusions all change simultaneously, and variations in the internal pressure of oil inclusions do not follow the isochore at the time the inclusions were trapped. Thus, T_{ho} changes according to the changes in the internal temperature, pressure and composition of the oil inclusions. The changes of oil composition, T_{ho} and F_{vo} after oil cracking have an important influence on the results of trapping pressure prediction using petroleum inclusion thermodynamics modeling (Ping et al., 2013). For example, if oil cracking increases the T_{ho}, the reconstructed P_t becomes lower than the initial trapping pressure of oil inclusions, and vice versa.

An increasing number of commercial oil and gas pools have been discovered in deeply buried reservoirs (DBRs) with depths greater than 3500–4000 m (Bloch et al., 2002; Bourdet et al., 2010; Wilkinson and Haszeldine, 2011). Numerous studies have drawn attention to crude oil thermal stability and oil compositional changes with increase in thermal stress (Behar et al., 2008; Hill et al., 2003; Price, 1993). Understanding the influences of crude oil cracking on the fluorescence color, homogenization temperature and trapping pressure of oil inclusions is important for reconstruction of oil and gas charging and accumulation histories using fluid inclusion data, especially in DBRs. However, experimental methods such as the synthesis of fluid inclusions cannot adequately explain the effects of oil cracking on fluorescence color and T_{ho} for two reasons. Firstly, the experimental temperature (generally greater than 300 °C) is much higher than the natural oil cracking temperature in the reservoir (generally from 150 to 250 °C), which may create a contrary result regarding fluorescence color changes during oil cracking compared to geological conditions. This occurs because of the reversed relative thermal stability of the C_{14+} saturates and aromatics between laboratory and geological conditions (Behar et al., 2008). For example, the C_{14+} saturates from a Type II oil are more stable under geological conditions than laboratory conditions (Behar et al., 2008), which could result in the saturate/aromatic ratio decreasing under laboratory conditions, while the ratio increases under geological conditions. Secondly, the low experimental pressures compared to high experimental temperatures result in lower P-T gradients (isochoric path) compared to natural reservoir conditions, which may give an incorrect trend of homogenization temperature.

The objective of this study is to demonstrate how the oil cracking process influences the fluorescence color, homogenization temperature and trapping pressure reconstruction of oil inclusions under subsurface reservoir conditions. Oil cracking kinetics modeling and petroleum inclusion thermodynamics modeling integrated with measured fluid inclusion data from DBRs in the northern Dongying Depression were used to decipher this process. The results may provide a theoretical constraint for reconstructing the oil and gas filling histories in DBRs by using natural fluid inclusion data.

2. Geological setting

The geological setting for the Dongying Depression was described in detail by Ping et al. (2017) and will be described only briefly here.

The Dongying Depression of the Jiyang Sub-basin lies in the southeastern Bohai Bay Basin (Fig. 1A), and is a typical Chinese Paleogene half graben faulted basin, covering an area of 5850 km^2. It is one of the most petroliferous rift areas in the Bohai Bay Basin (Li, 2004). This depression is bounded by the Chenjiazhuang High to the north, the Qingtuozi High to the east, the Luxi Uplift and Guangrao High to the south, and the Qingcheng High to the west (Fig. 1B). The depression can be divided into five secondary tectonic zones from the north to south (Fig. 1B). The northern Dongying Depression is located between the northern steep slope zone and central uplift zone of the Dongying Depression, including the Lijin, Shengtuo, and Minfeng areas (Fig. 1C).

The Cenozoic strata of the northern Dongying Depression are distributed widely in the basin and have a maximum thickness of more than 7000 m, and are the primary sediments for oil and gas generation and accumulation (Yong, 2006). The strata consist of the Paleogene Kongdian (Ek), Shahejie (Es) and Dongying (Ed) formations, and the Neogene Guantao (Ng) and Minghuazhen (Nm) formations. The Shahejie Formation can be further subdivided from top to bottom into Member I (Es_1), Member II (Es_2), Member III (Es_3) and Member IV (Es_4). The Es_4 member is also divided into the upper sub-member of Member IV (Es_4^U) and the lower sub-member of Member IV (Es_4^L). In this study, the DBRs are mainly distributed in the Es_4^L sub-member in the northern Dongying Depression.

As a part of the Bohai Bay Basin, the Mesozoic-Cenozoic tectonic history of Dongying Depression developed in three stages (Allen et al., 1997; Chang, 1991; Yong, 2006). 1) A pre-rift stage happened during the Triassic thru Early Cretaceous, when a series of grabens and half grabens developed along major NW and NE-trending fault sets, and the rudiments of a rifted basin formed. Afterwards, uplift and erosion occurred during Late Cretaceous thru Paleocene. 2) A Paleogene syn-rift stage was characterized by fault

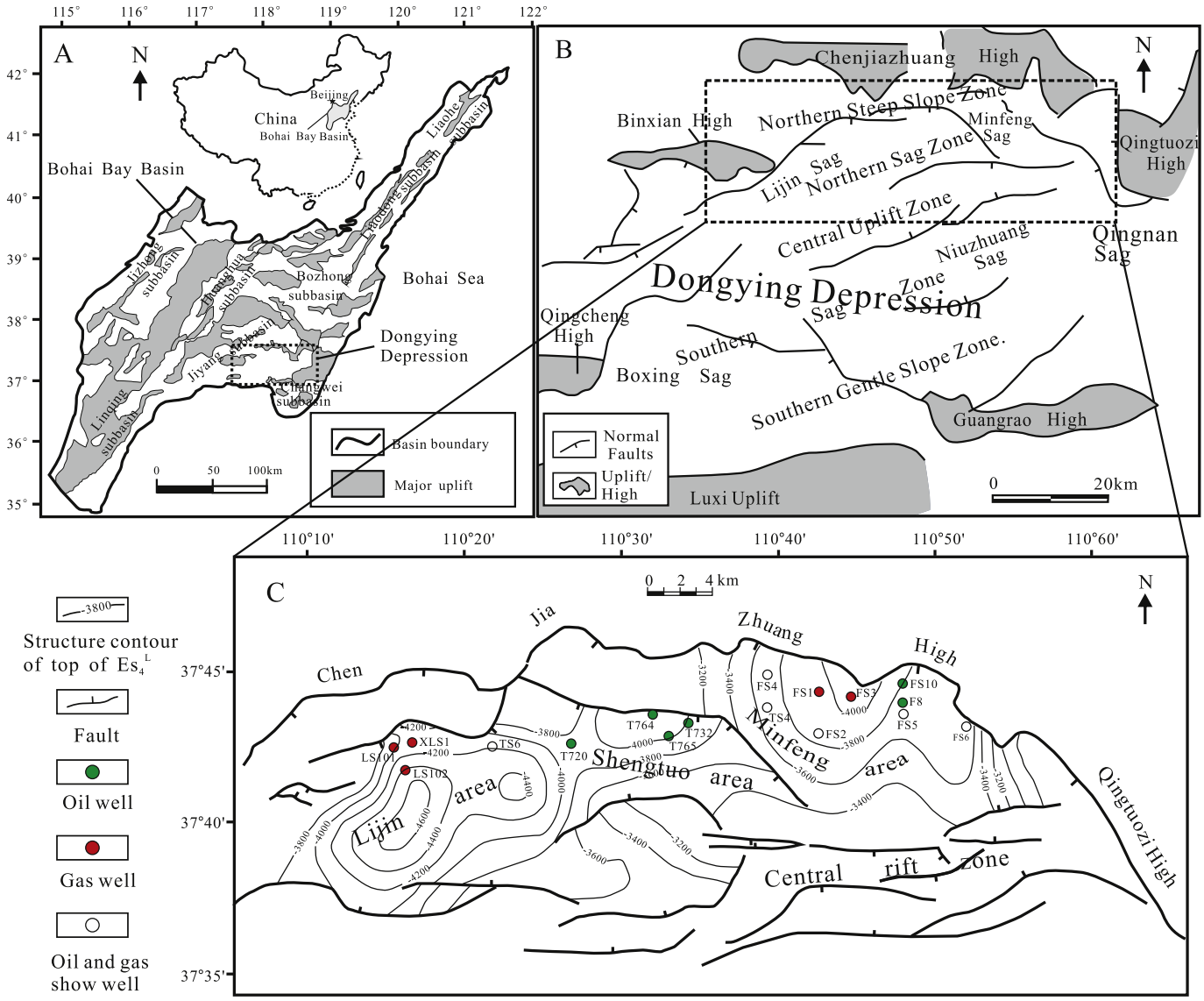

Fig. 1. (A) Location of the Dongying Depression relative to the Bohai Bay Basin; (B) Maps showing elementary structural features in Dongying Depression; (C) Locations of oil and gas wells in the study area in the northern Dongying Depression.

block extension, basin expansion, rapid deposition and intense tectonic activities. 3) A post-rift stage happened during the Neogene thru Quaternary, when fluvial and floodplain sediments developed.

In recent years, several oil and gas reservoirs have been found in the Lijin, Shengtuo and Minfeng areas in the DBRs in the northern Dongying Depression (Fig. 1C), which was an important breakthrough for oil and gas exploration. Geochemical evidence supports the Es_4^L sub-member's dark mudstone as the main hydrocarbon source rock (Ding et al., 2011; Wang, 2009). The oil and gas reservoirs are characterized by high temperatures and high pressures (HTHP) and great burial depth (3500–4500 m). However, what is more interesting is that the oil and gas reservoirs exhibit variable petroleum types and pressure systems in the three different fields (Lijin, Shengtuo and Minfeng fields). The Lijin field is characterized by HTHP gas-condensate reservoirs, the Shengtuo field is characterized by HTHP oil reservoirs, and the Minfeng field is characterized by high temperature, hydrostatic pressure gas-condensate reservoirs (Fig. 2). Please refer to Ping et al. (2017) for more information on the types of hydrocarbon fluids and pressure-temperature (P-T) conditions of the DBRs in the northern Dongying Depression.

3. Methods

3.1. Fluid inclusion analysis

The various pressure systems and formation temperatures in the DBRs of the Dongying Depression facilitate the comparison of the effects of pressure and temperature on oil cracking to understand the temperature ranges at which the T_{ho} and fluorescence color of oil inclusions are affected by oil cracking, and whether the effects depend on the pressure conditions (hydrostatic pressure or overpressure) when the oil inclusions were trapped. Therefore, several wells were selected to perform fluid inclusion measurements, including fluorescence spectroscopy and microthermometry, from the Shengtuo area and Minfeng area at burial depths from 3672 m to 4359 m (140 °C-185 °C) and pressure systems from normal pressure (Minfeng area) to overpressure (Shengtuo area) (Fig. 2).

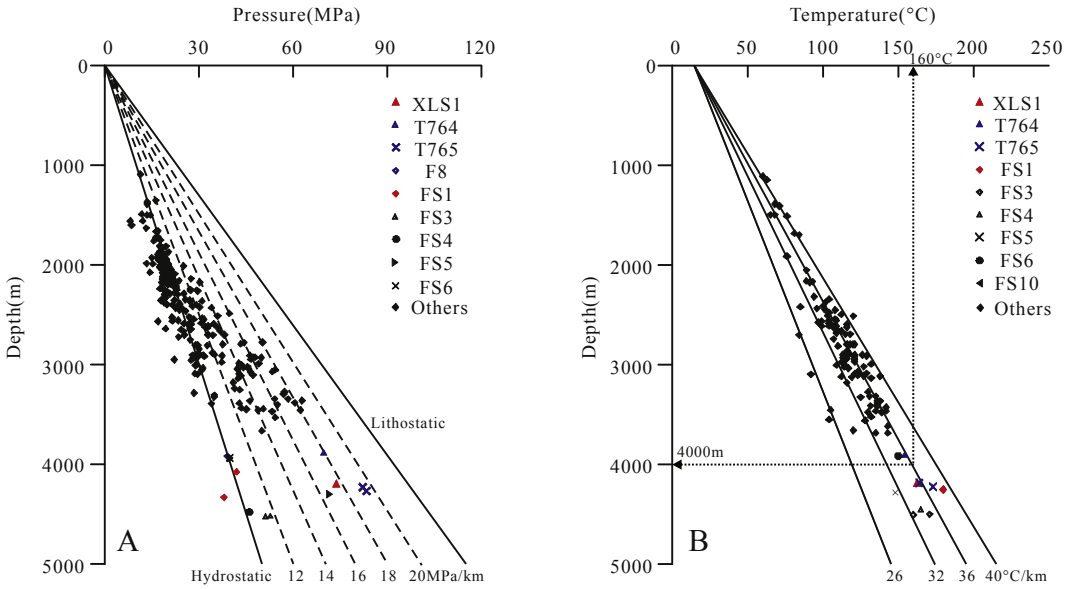

Fig. 2. Pressure-depth plot (A) and temperature-depth plot (B) for wells in the northern Dongying Depression.

Thirty-four sandstone and vein core samples from six wells were prepared as double-polished thin sections for fluid inclusion analysis. Petroleum inclusions were identified under illumination with ultraviolet (UV) light, and the visual fluorescence colors were determined and classified as yellow, blue-white and blue, which may be related to increasing thermal maturity (George et al., 2001, 2002; Oxtoby, 2002). Because of the low resolution and controversy associated with maturity assessment of petroleum inclusions with visual fluorescence colors, and because of human bias in color perception (Oxtoby, 2002), fluorescence spectroscopy during illumination with UV light was undertaken. The parameters measured were the λ_{max} (wavelength of the maximum intensity), $Q_{650/500}$ (ratio of the intensity at 650 nm to the intensity at 500 nm) and QF-535 values (ratio of the 535–750 nm flux to the 430–535 flux), in order to characterize the composition of the oil inclusions (Munz, 2001).

Microthermometry of petroleum inclusions and aqueous inclusions was carried out using a Linkam THMS 600 heating-freezing stage that was attached to a Nikon 80I microscope. Fluid inclusions that showed obvious signs of necking-down, leakage or stretching were not measured by microthermometry (Goldstein, 2001). The fluorescence spectroscopy of individual petroleum inclusions was measured before performing the microthermometry, and T_{ha} was determined before freezing runs to avoid the effects of stretching during freezing on T_{ha} (McLimans, 1987). Furthermore, the T_{ho} was measured before homogenization of the aqueous inclusions (Munz, 2001). When the T_h exceeded 180 °C, which corresponds to the estimated maximum formation temperatures that were experienced by the host samples, the fluid inclusions trapped in healed fractures in quartz were selected for measurement with great care, as the origin of the fluid inclusions was unknown.

3.2. Kinetic modeling of crude oil cracking

The kinetics of crude oil cracking have been widely used to quantitatively evaluate compositional changes with increasing thermal stress (Behar et al., 2008; Kuo and Michael, 1994; Tsuzuki et al., 1999; Ungerer et al., 1988). Crude oil cracking is controlled by the kinetics of cracking reactions, which can be adequately described using simple first-order kinetics (Tissot and Espitalié, 1975) or a set of parallel first-order reactions (Behar et al., 2008; Kuo and Michael, 1994; Tsuzuki et al., 1999; Ungerer et al., 1988).

This study quantitatively predicts changes in components based on the kinetic modeling of crude oil cracking and calculates the internal pressure and volume varieties of oil inclusions during oil cracking, which usually requires more detailed composition contents in the oil (e.g., components range from methane (C_1) to heptane plus (C_{7+})) to obtain more accurate predictions of P-T phase diagrams and the volume of crude oil (Ping et al., 2011, 2013). Therefore, a more detailed compositional model for both cracking kinetic modeling and P-T thermodynamics modeling is necessary. The oil cracking component model in this study is divided into the following twelve components according to Vandenbroucke et al. (1999): CO_2 (non-hydrocarbon gas), C_1 (hydrocarbon gas), C_2 (hydrocarbon gas), $C_{3\text{-}5}$ (hydrocarbon gas), $C_{6\text{-}13}$ SAT (light saturated hydrocarbons), $C_{6\text{-}13}$ ARO (light aromatic hydrocarbons), C_{14+} SAT (heavy saturated hydrocarbons), C_{14+} ARO C (condensed ring aromatic hydrocarbons), C_{14+} ARO U (unstable heavy aromatics), C_{14+} NSO (non-hydrocarbon components), precoke (pyrobitumen predecessor) and coke (pyrobitumen). Assuming that CO_2, CH_4 and pyrobitumen cannot be cracked, the cracking process of the above twelve components can be described with nine parallel first-order kinetics reactions. The chemical reaction rate constant follows the Arrhenius equation:

$$K_{ij} = A_{ij} exp\left(\frac{-E_{ij}}{RT}\right) \quad (1)$$

In Eq. (1), A_{ij}, E_{ij}, R and T represent the frequency factor (pre-factor), activation energy, gas constant and reaction temperature, respectively.

Once the oil cracking model is defined, the component changes during oil cracking under different thermal evolution conditions can be calculated based on kinetic parameters, such as the activation energy (E), frequency factor (F) and stoichiometric coefficient, and the initial crude oil composition and thermal evolutionary history after the oil inclusions were trapped. The oil cracking model and kinetic parameters that are used in this study are from Vandenbroucke et al. (1999), except the kinetic parameters for ethane cracking are from Kuo and Michael (1994) (Table 1).

Table 1
Crude oil cracking kinetic modeling parameters used in this study.

Composition	lnA (s^{-1})	E (kcal/mol)	CO_2 (wvt %)	C_1 (wt %)	C_2 (wt %)	C_{3-5} (wt %)	C_{6-13} SAT (wt %)	C_{6-13} ARO (wt %)	C_{14+} SAT (wt %)	C_{14+} ARO C (wt %)	C_{14+} ARO U (wt %)	C_{14+} NSO (wt %)	Precoke (wt %)	Coke (wt %)	Reference
C_2	48.25	80.0		3.4		95.9	0.7								Kuo and Eric Michael (1994)
C_{3-5}	32.55	65.8		40.0	18.8			41.2							Vandenbroucke et al. (1999)
C_{6-13}SAT	32.55	60.3		11.1	15.7	36.2		37.0							Vandenbroucke et al. (1999)
C_{6-13}ARO	27.70	56.5		13.2						69.0			17.8		Vandenbroucke et al. (1999)
C_{14+}SAT	40.95	68.0		2.7	2.7	5.4	55.3	28.5			5.4				Vandenbroucke et al. (1999)
C_{14+}ARO C	27.70	54.5		12.0									88.0		Vandenbroucke et al. (1999)
C_{14+} ARO U	32.55	57.0		3.0	5.0	10.0	12.0	10.0	15.0	10.0			35.0		Vandenbroucke et al. (1999)
C_{14+}NSO	32.55	54.9	15.0	2.2	0.9	2.2	11.1	3.7	13.3		6.0		45.6		Vandenbroucke et al. (1999)
Precoke	32.55	64.4	9.4	4.7	0.3									85.6	Vandenbroucke et al. (1999)

3.3. Thermodynamics modeling of oil inclusions

The physical significance of T_{ho} and the determination of T_{ho} after oil cracking are shown in Fig. 3. An oil inclusion with known composition was trapped at point C_1 (P_{t1}, T_{t1}), from which the isochore (line C_1B_1) can be determined (Aplin et al., 1999; Ping et al., 2013). As the temperature decreases, the internal pressure decreases along line C_1B_1 until the isochore intersects the bubble point curve $L(G)_1$ at point B_1. The temperature at point B_1 represents the trapped T_{ho} at point C_1. With increase of formation temperature after trapping, the internal pressure will increase following the isochore C_1B_1 if the oil composition and volume of oil inclusion do not change. However, crude oil cracking occurs once the oil inclusion experiences much higher thermal stress after trapping (T_{t2}), which directly results in changes in the composition and P-T phase diagram ($L(G)_2$ and $G(L)_2$) and the internal pressure of the oil inclusion (P_{t2}). As the T_{ho} greatly depends on the composition and isochore of the oil inclusion (Aplin et al., 1999; Ping and Chen, 2011; Ping et al., 2013), the initial P-T trapping conditions (P_{t1}, T_{t1}) of the oil inclusion are revised to the new P-T trapping conditions (P_{t2}, T_{t2}) and a new isochore (line C_2B_2), which changes T_{ho1} and F_{vo1} into T_{ho2} and F_{vo2}. Please note that Fig. 3 is a schematic drawing of new P-T trapping conditions of an oil inclusion after oil cracking. How the phase diagram and isochore of the oil inclusion changes depends on the oil composition and internal pressure in oil inclusion.

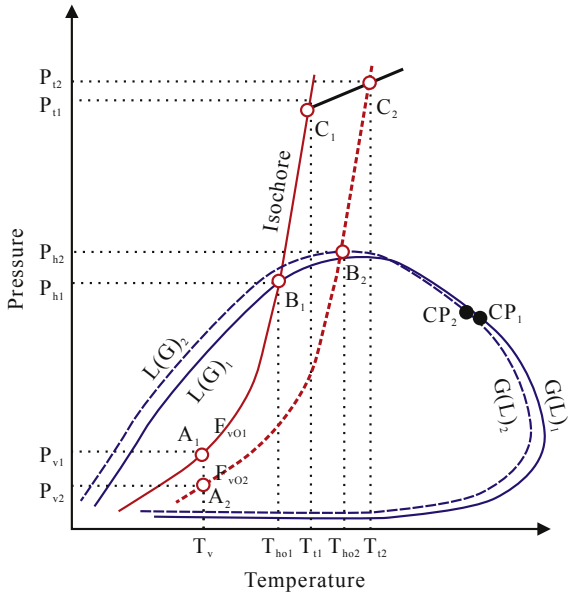

Fig. 3. Typical pressure-temperature (P–T) phase diagram of a petroleum initially trapped as an oil inclusion (Oil 1). The liquid-gas immiscibility loop is delimited by the bubble point line ($L(G)_1$) and the dew point line ($G(L)_1$), joining at the critical point (CP_1). The P-T path of the inclusion is described by an isochore, whose three points are of importance: the (P_{t1}, T_{t1}) trapping point C_1, the (P_{h1}, T_{ho1}) homogenization point B_1, and the (P_{v1}, T_{v1}) point A1, at which the bubble filling degree (F_{vo1}) is measured. The P-T phase diagram changes to Oil 2 with the variation of oil composition because of oil cracking at the formation temperature, T_{t2}, which results in the synchronous changes in internal pressure (P_{t2}), homogenization temperature (T_{ho2}) and the bubble filling degree (F_{vo2}), defined by the dashed lines showing the liquid-gas immiscibility loop and the isochore, and the points CP_2, C_2, B_2 and A_2.

According to Fig. 3, three conditions must be satisfied when calculating the T_{ho}: 1) the oil inclusion components must be accurately obtained; 2) the P-T phase diagram of the known oil components must be accurately calculated; and 3) the isochore line must be accurately calculated under the formation temperature and internal pressure of the oil inclusion during oil cracking. The changes in components during oil cracking can be calculated through oil cracking kinetic modeling, and the P-T phase diagram can be calculated by the equation of state (Peng and Robinson, 1976). Solid pyrobitumen (coke) and pyrobitumen predecessor (precoke) are produced during oil cracking and are insoluble in liquid hydrocarbons (Behar et al., 1992), which can lead to changes in the liquid volume and internal pressure, while the internal pressure determines the isochore line of the oil inclusion if the formation temperature and composition are known.

Once the oil inclusion components and internal pressure have been determined, the P-T phase diagram, isochore line, T_{ho}, and F_{vo} can be determined (Fig. 3). To ensure that the calculations of the oil inclusion's isochore line and F_{vo} are accurate, this study calculates the gas and liquid molar volume by using the volume translation method, through which the prediction accuracy of the isochore line and F_{vo} can be improved (Ping et al., 2013). After obtaining the changes in T_{ho} during oil cracking, the trapping pressure of the oil inclusion is reconstructed based on the oil components, T_{ho} after oil cracking, and the trapping temperature (Fig. 3), so as to compare the effect of oil cracking on the accuracy of the trapping pressure prediction of the oil inclusion.

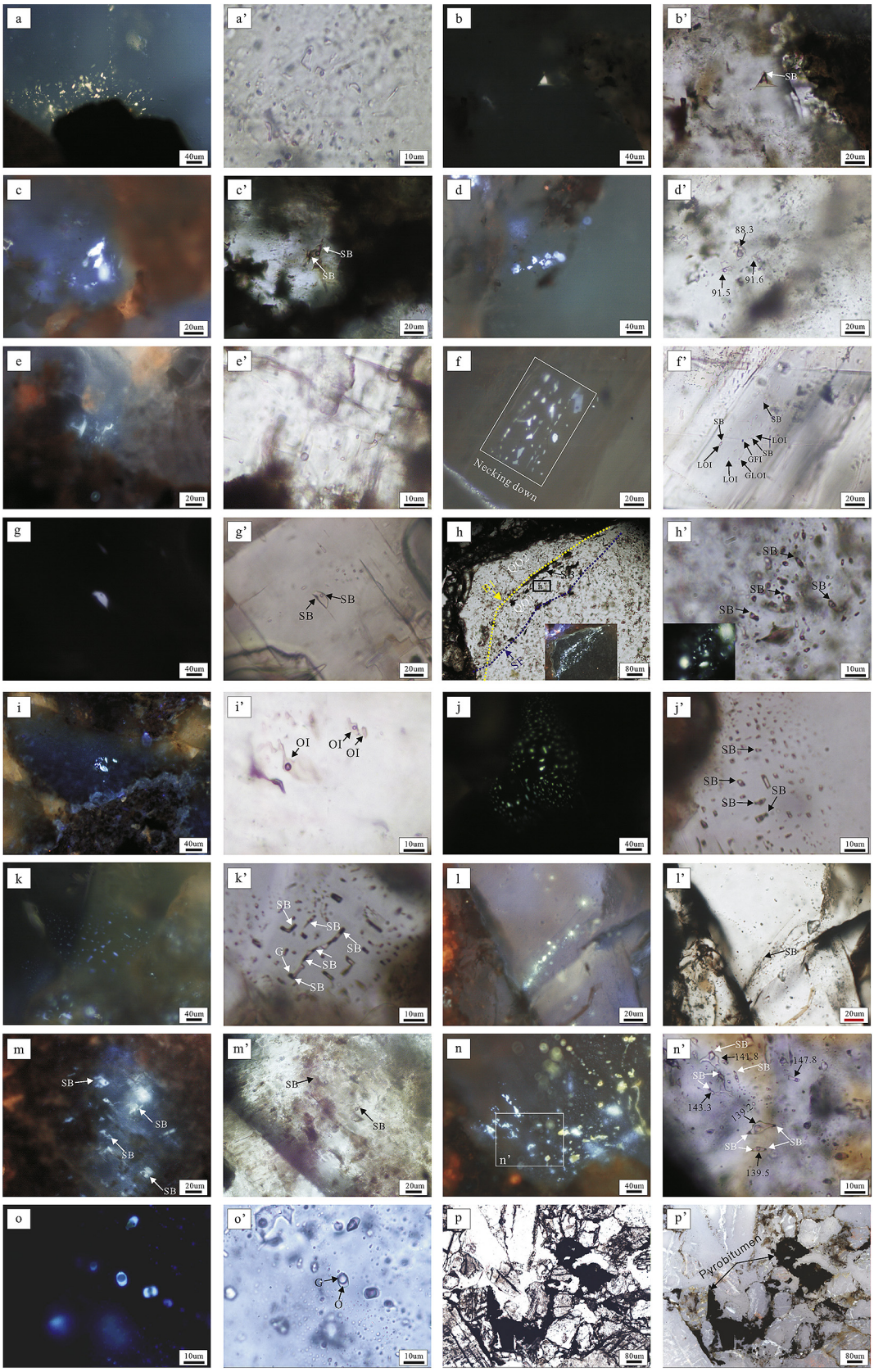

Fig. 4. Photomicrographs of oil inclusions and pyrobitumen in the DBRs of the northern Dongying Depression. Photomicrographs a, b, c, d, e, f, g, i, j, k, l, m, n, o, p were taken under visible fluorescence with ultraviolet excitation, and others were taken under transmitted light. Abbreviations: GLOI = gas-liquid phase oil inclusion under room temperature; LOI = pure liquid phase oil inclusion under room temperature; GFI = pure gas phase fluid inclusion under room temperature; OI = oil inclusion; O = oil; G = gas; SB = solid bitumen; QO1 = the first stage of quartz overgrowth; QO2 = the second stage of quartz overgrowth; B1 = the boundary of the QO1 and the QO2; SF = the secondary fracture crossing the QO2. Note that it is very difficult to distinguish bitumen from pyrobitumen in the fluid inclusions, so the term "solid bitumen" was used in the following sections

4. Results and discussion

4.1. Fluorescence characteristics and T_{ho} of oil inclusions in DBRs

4.1.1. Fluorescence colors

Oil inclusions from 3677.7 m in well T732 show yellow fluorescence color (Fig. 4a), and no visible solid bitumen can be detected in the oil inclusions under transmitted light (Fig. 4a′). Oil inclusions from 3951.8 m, 3952.9 m and 3958.5 m in well T764 mostly occurred in secondary trails in detrital quartz grains as two-phase vapor-liquid inclusions with light-yellow to blue-white fluorescence colors under UV light (Fig. 4b-b′ and Fig. 4c-c′). Solid bitumen was observed in both light-yellow fluorescent oil inclusions (Fig. 4b-b′) and blue-white fluorescent oil inclusions (Fig. 4c-c′), which suggests that thermal cracking of the oil in the oil inclusions could have occurred. Blue-white fluorescence color oil inclusions were detected in a quartz vein from 4358.5 m in well T765 under UV light (Fig. 4d). These inclusions are two-phase liquid-vapor, colorless inclusions at room temperature with a large vapor-liquid volume ratio, and no obvious solid bitumen was observed (Fig. 4d′). The nearly consistent T_{ho} values in the same fluid inclusion assemblage indicates that the oil inclusions with large F_{vo} were trapped as a single homogeneous fluid (Fig. 4d′).

Abundant oil inclusions from well F8 in the Minfeng area have been observed in a calcite vein at 3943.0–3943.2 m. The majority of the oil inclusions in these samples are two-phase liquid-vapor inclusions at room temperature, with small vapor-liquid volume ratios, no color under transmitted light and blue-white (Fig. 4e and f) or light-yellow fluorescence colors (Fig. 4g) under UV light. The size of these inclusions are often greater than ten micrometers, and they have elongated and irregular shapes (Fig. 4f). These inclusions were trapped in a group along the cleavage plane of calcite and are interpreted to be primary (Fig. 4f). Various fluid phases occur in the same fluid inclusion assemblage; some oil inclusions are pure liquid-phase or pure gas-phase fluid inclusions, and some exhibit two-phase gas-liquid inclusions (Fig. 4f and f′). These oil inclusions were interpreted to be the result of necking-down after a phase change (see Fig. 4f and f′ for an explanation), as shown by the presence of multiple phases of fluid inclusions, and two inclusions that are adjoined by a neck (Goldstein, 2001). In addition, solid bitumen occasionally occurs in some single-phase liquid oil inclusions or in two-phase gas-liquid oil inclusions (Fig. 4f and f′). This observation suggests that the solid bitumen was generated before the necking-down, otherwise solid bitumen would occur throughout the same fluid inclusion assemblage.

Blue-white fluorescence color oil inclusions from a sandstone at 4195.1 m in well F8 have been detected in interior quartz overgrowths (QO1 in Fig. 4h), the boundary of two episodes of quartz overgrowths (QO1 and QO2) (B1 in Fig. 4h), and a secondary healed fracture that transects quartz overgrowths (SF in Fig. 4h). The oil inclusions in the secondary healed fracture (SF) contain little solid bitumen and have similar vapor-liquid volume ratio. However, black non-fluorescent solid bitumen has been observed in the corner of inclusion walls, and identical solid-liquid volume ratios indicate solid bitumen in the oil inclusions in the QO1 and B1 (Fig. 4h′), which may have been generated by thermal cracking after oil inclusion trapping. The absence of solid bitumen in the oil inclusions within the SF suggests that these oil inclusions could have experienced relatively weak oil cracking, because these oil inclusions were trapped later than those trapped in QO1 and B1, and thus would have experienced less heating time. Furthermore, it has been noticed that the oil inclusions within QO1, B1 and SF have consistent blue-white fluorescence colors, possibly due to oil cracking which may have changed the original oil compositions in the oil inclusions and thus shifted the fluorescence color.

Blue-white fluorescent oil inclusions were detected in the healed fractures of detrital quartz in well FS1 (3684.9 m) and contain no obvious black solid bitumen in the inner walls of the oil inclusions (Fig. 4i). The blue-white fluorescent oil inclusions trapped within a calcite crystal in a calcite vein from well FS1 (4023.5 m) also have variation in the proportion of fluid phases, and pairs of oil inclusions with necks joining them, which suggests that the oil inclusions have been necked down (Fig. 4k and k′). However, both yellow (Fig. 4j) and blue-white fluorescent (Fig. 4k) oil inclusions from 4023.5 m in well FS1 generally contain black solid bitumen in the corner of the oil inclusions, supporting the hypothesis that the solid bitumen was formed after the necking-down event and therefore is most likely related to increasing thermal stress.

Oil inclusions from 4321.7 to 4323.6 m in well FS1 show varying fluorescence colors under UV light, from light yellow to blue-white and blue. The light-yellow (Fig. 4l and l′) and blue-white fluorescent inclusions (Fig. 4m and n) are liquid-dominated liquid-vapor inclusions, and the blue fluorescent inclusions (Fig. 4o and o′) are vapor-dominated liquid-vapor inclusions. These inclusions generally occur in healed cracks in quartz and feldspar grains. The light-yellow fluorescent inclusions show light-yellow color under transmitted light and usually have small vapor-liquid volume

regardless of its origin. (a-a′) Yellow fluorescence color oil inclusions trapped within the healed fractures in detrital quartz from well T732 (3677.7 m) showing no visible black solid bitumen in oil inclusions. (b-b′) Single yellow fluorescence color oil inclusion trapped within the healed fractures in detrital quartz from well T764 (3952.9 m) showing black solid bitumen in the corner and in the inner wall of the oil inclusion. (c-c′) Blue-white fluorescence color oil inclusions trapped within the healed fractures in detrital quartz from well T764 (3951.8 m) showing black solid bitumen with a similar bitumen volume ratio in the inner wall of the oil inclusions. (d-d′) Blue-white fluorescence color oil inclusions trapped within a quartz vein from well T765 (4358.49 m), showing no obvious black solid bitumen in the inner walls of the oil inclusions. Note that the F_v of the oil inclusions are large, and the T_{hs} are similar (the numbers in d′). (e-e′) Blue-white fluorescence color oil inclusions within a calcite crystal in a calcite vein from well F8 (3943.2 m), showing no obvious black solid bitumen in the inner wall of the oil inclusions. (f-f′) White fluorescence color oil inclusions within a calcite crystal in a calcite vein from well F8 (3943.0 m), showing necking-down of oil inclusions. Note the obvious black solid bitumen in the inner wall of some of the oil inclusions. (g-g′) White fluorescence color oil inclusion within a calcite crystal in a calcite vein from well F8 (3943.0 m), showing obvious black solid bitumen in the inner wall of the oil inclusion. (h) Two stages of quartz overgrowth (QO1 and QO2) occur in a sandstone from well F8 (4195.1 m). Insets show photomicrographs of the same field-of-view taken under ultraviolet excitation. Blue-white fluorescence color oil inclusions are trapped within the QO1, the boundary (B1) of QO1 and QO2, and the secondary healed fracture (SF) cutting the QO2. (h′) Blue-white fluorescence color oil inclusions within the QO1 have nearly identical volume ratios of oil/gas/bitumen, indicating that the oil was a homogeneous liquid at the time of quartz overgrowth and fluid entrapment, and the solid bitumen was generated after the trapping of oil. (i-i′) Blue-white fluorescence color oil inclusions trapped in the healed fracture of detrital quartz in well FS1 (3684.9 m), showing no obvious black solid bitumen in the inner wall of the oil inclusions. (j-j′) Yellow fluorescence color oil inclusions trapped within a calcite crystal in a calcite vein from well FS1 (4023.5 m), showing an identical bitumen volume ratio. (k-k′) Blue-white fluorescence color oil inclusions trapped within a calcite crystal in a calcite vein from well FS1 (4023.5 m), Note that solid bitumen can be seen in the inner wall of the oil inclusions. (l-l′) Yellow fluorescence color oil inclusions with solid bitumen in the inner wall trapped in the healed fracture of a detrital quartz grain in well FS1 (4321.7 m). (m-m′) Blue-white fluorescence color oil inclusions with obvious solid bitumen in the inner wall trapped in the healed fracture of a detrital feldspar grain in well FS1 (4322.0 m). (n-n′) Blue-white fluorescence color oil inclusions trapped in the healed fracture of a detrital quartz grain in well FS1 (4321.7 m), showing nearly identical volume ratios of oil/gas/bitumen and T_{hos} (numbers in n′). The inset in n shows the expansion in n′. (o-o′) Blue fluorescence color gas condensate fluid inclusions trapped in the healed fracture of a detrital quartz grain in well FS1, showing no solid bitumen in the inner wall of the oil inclusions. (p-p′). Pyrobitumen was observed in the intergranular pore of the sandstone sample at 4321.7 m in well FS1. (For interpretation of the references to colour in this figure legend, the reader is referred to the web version of this article.)

ratios. The blue-white and blue fluorescent inclusions are colorless under transmitted light with uniform and large vapor-liquid volume ratios. Black solid bitumen (Fig. 4l′, m′ and n′) can be observed in the corners of the yellow and blue-white fluorescent oil inclusions, but not in the blue fluorescent oil inclusions.

Three lines of evidence suggest that oil cracking has occurred in oil inclusions from 4321.7 to 4323.6 m in well FS1: 1) the measured high formation temperatures (185 °C), under which the NSO compositions in oil are significantly cracked (Behar et al., 2008); 2) the consistent volume ratios of solid bitumen to oil inclusions and T_{ho} values (Fig. 4n′) indicate that the solid bitumen originated from the thermal cracking of oil after being trapped as fluid inclusions; and 3) non-fluorescent pyrobitumen filling was found in intergranular pores (Fig. 4p and p′).

4.1.2. Fluorescence spectroscopy

The UV fluorescence spectroscopy of a large number of oil inclusions from the DBRs in the northern Dongying Depression and other sags in the Dongying Depression have been examined to monitor the fluorescence spectroscopy parameter changes with increasing depth. Fig. 5 shows the distributions of λ_{max}, $Q_{(650/500)}$, and QF-535 at depths from 1500 m to 4500 m. Generally, four types of oil inclusions with different thermal maturities can be recognized according to their λ_{max} values (Fig. 5A). The least mature oil inclusions have λ_{max} ranging from 570 to 595 nm, and were only detected at depths between 2500 m and 3050 m in the South Niuzhuang Slope of the Dongying Depression. This type of oil inclusion is characterized by orange-red fluorescence, which could indicate a larger percentage of C_{14+} NSO and C_{14+} ARO compositions (George et al., 2001). The presence of this least-mature fluid inclusion assemblage is consistent with the discovery of "immature oils" in the South Niuzhuang Slope (Pang et al., 2003). The most common oil inclusions contain mature oil that is characterized by yellow fluorescence, with the main λ_{max} ranging from 530 to 549 nm. This type of mature oil inclusion has been detected over the entire Dongying Depression over a wide range of depths from 1500 m to 4000 m.

The other two types of oil inclusions are more mature. Although these more mature oil inclusions have been measured across the entire depth range, they were mainly detected in the DBRs in the northern Dongying Depression, and only the more mature oil inclusions were detected below 4000 m. This type of oil inclusion is characterized by blue-white and blue fluorescence with black solid bitumen in the corner or the wall of the oil inclusions (Fig. 4). Most of the oil inclusions have a λ_{max} value between 530 nm and 549 nm above 4000 m, but all the oil inclusions have a λ_{max} value < 500 nm below 4000 m. Theoretically, different oil maturities over the entire oil generation stage should be detected, and the maturity of the oil inclusions in deeper reservoirs should not be constrained (λ_{max} < 500 nm). One possible explanation is that the source rock for the oil in the deeper formations only generated oil with λ_{max} < 500 nm, or only oil inclusions with high thermal maturity were trapped. This interpretation does not make much sense because it is impossible that all the samples below 4000 m did not record the less mature oil charges (λ_{max} > 500 nm), which are responsible for shallower oil accumulations. Therefore, these findings are interpreted to be the result of the thermal cracking of oil, as shown by the universal presence of solid bitumen in the same fluid inclusion assemblage below 4000 m.

4.1.3. T_{ho} of oil inclusions

Two wells (wells F8 and FS1) from the Minfeng area and three wells (wells T720, T764 and T765) from the Shengtuo area (Fig. 1C), which have depths that range from 3672 m to 4358 m, were selected to investigate the T_h distributions of oil inclusions with changes in burial depth. The T_{ha} and T_{ho} values are shown in Fig. 6.

Fig. 6A shows the T_h distributions of oil inclusions and aqueous inclusions from 3672 m in well T720. The yellow fluorescing oil inclusions have measured T_h between 79 °C and 91 °C (Fig. 6A), while the oil inclusions from 3951.8 m to 3952.9 m in well T764 show broad T_h values in the histogram (Fig. 6B), ranging from 60 °C to 150 °C for inclusions that were trapped in healed fractures in feldspars. Oil inclusions with blue-white fluorescence from quartz veins in 4358.5 m sandstone from well T765 have measured T_h between 80 °C and 115 °C, with most in the 80–95 °C range and others spread between 100 °C and 115 °C (Fig. 6C).

Oil inclusions with yellow and blue-white fluorescence from 3943.0 m in well F8 have measured T_h between 40 °C and 75 °C,

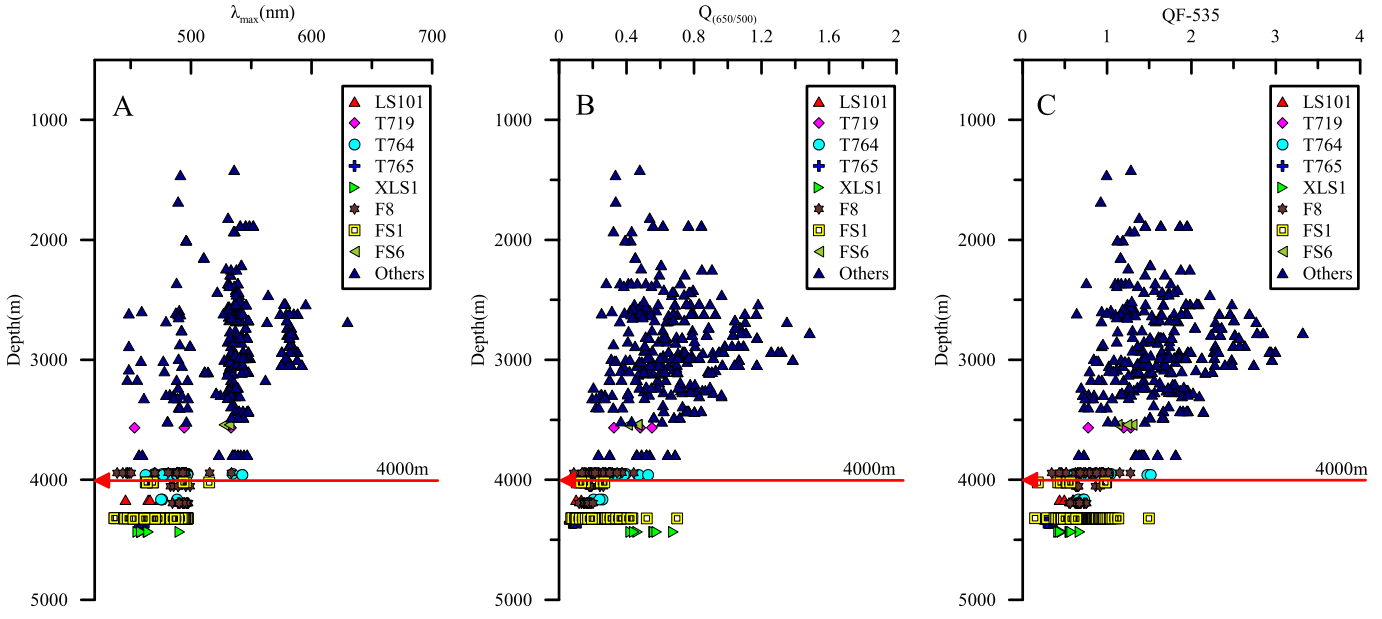

Fig. 5. Variations of fluorescence spectroscopy parameters of oil inclusions with depth in the studied Dongying Depression wells: λ_{max} (A), $Q_{(650/500)}$ (B) and QF-535(C). Note that "others" in the legend are the fluorescence spectroscopies of oil inclusions from other areas in the Dongying Depression.

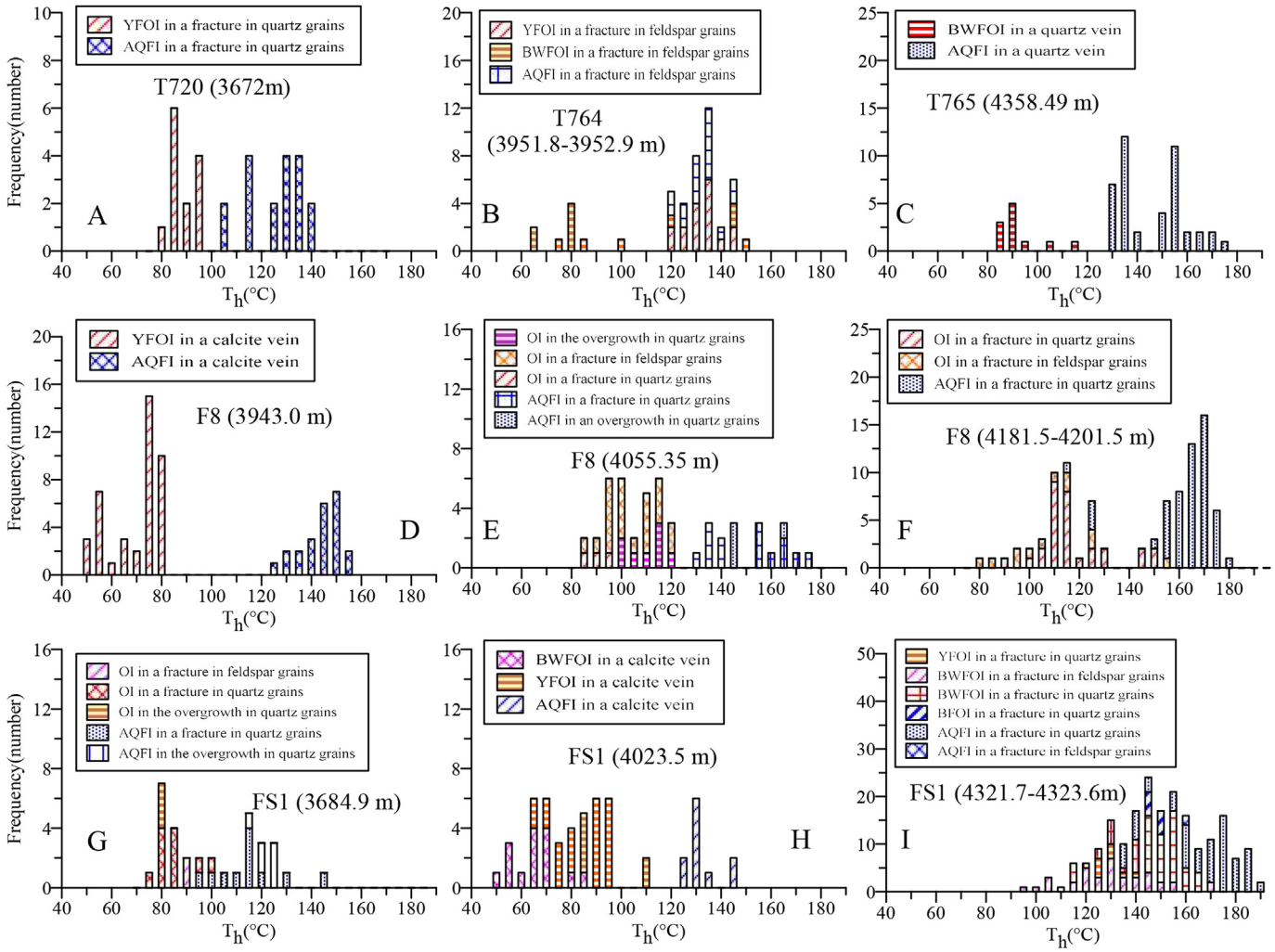

Fig. 6. T_h distributions of fluid inclusions from (A) wells T720 (3672 m), (B) T764 (3951.8–3952.9 m), (C) T765 (4358.49 m), (D) F8 (3943.0 m), (E) F8 (4055.35 m), (F) F8 (4181.5–4201.5 m), (G) FS1 (3684.9 m), (H) FS1 (4023.5 m), and (I) FS1 (4321.7–4323.6 m) in the DBRs of the Dongying Depression. AQFI: aqueous fluid inclusion; BWFOI: blue-white fluorescing oil inclusion; YFOI: yellow fluorescing oil inclusion; OI: oil inclusion. (For interpretation of the references to colour in this figure legend, the reader is referred to the web version of this article.)

with most in the 65–75 °C range (Fig. 6D). Oil inclusions from 4055.35 m in well F8 were trapped within healed fractures in quartz and feldspar grains and in quartz overgrowths, which have measured T_h between 83 °C and 116 °C, with two modes at 90–100 °C and 105–115 °C, respectively (Fig. 6E). The T_h values of oil inclusions from 4195.2 m in well F8 show a wide distribution from 75 °C to 155 °C, with most in the 105–115 °C range (Fig. 6F). The T_h of oil inclusions with solid bitumen that were trapped within QO1 (Fig. 4h′) and in the boundary (B1 in Fig. 4h) between QO1 and QO2 could not be measured.

Oil inclusions from 3684.9 m in well FS1 were trapped within healed fractures in quartz and feldspar grains and in quartz overgrowths, which have measured T_h between 70 °C and 110 °C, with most in the 75–85 °C range (Fig. 6G). Oil inclusions that were trapped in a calcite vein from 4023.5 m show a wide distribution of T_h from 45 °C to 110 °C (Fig. 6H). Blue-white fluorescing oil inclusions have measured T_h between 45 °C and 85 °C, with two major modes at 50–55 °C and 60–70 °C. The T_h values of yellow fluorescing oil inclusions are generally higher, and range from 65 °C to 110 °C with a mode at 85–95 °C. Oil inclusions with yellow, blue white and blue fluorescence from 4321.7 to 4323.6 m in well FS1 have measured T_h values between 95 °C and 175 °C, with most in the 125–160 °C range (Fig. 6I).

In summary, the T_{ho} of oil inclusions from wells F8 and FS1 increases with burial depth, but the oil inclusions from Shengtuo area show different trends depending on their fluorescence color. The yellow fluorescing oil inclusions have increasing T_{ho} from 3672 m to 3952.9 m, while the blue-white fluorescing oil inclusions have a similar T_{ho} range from 3951.8 m to 4358.49 m.

4.2. Modeling variations in the composition and T_h of oil inclusions during oil cracking

4.2.1. Assumptions

The oil cracking process is very complex, so many variables are not known. Some preconditions should be satisfied before calculating the internal pressure and T_{ho} during oil cracking by using petroleum inclusion thermodynamics modeling:

(1) The bulk volume of the oil inclusion, including solid pyrobitumen and pyrobitumen predecessor, does not change during oil cracking;
(2) No fluids are input into the oil inclusion, nor does leaking occur from the oil inclusion during oil cracking;

Table 2
The initial composition contents of oil inclusions used for oil cracking process modeling (molecular weight are from Hantschel and Kauerauf (2009)).

Composition	Molecular weight (g/mol)	Oil inclusion A		Oil inclusion B	
		Molar percentage (mol%)	Weight percentage (wt.%)	Molar percentage (mol%)	Weight percentage (wt.%)
C_1	16.00	34.7	5.2	47.9	9.6
C_2	30.07	6.5	1.8	7.9	3.0
C_3	44.10	6.1	2.6	6.0	3.3
iC_4	58.12	1.4	0.8	1.2	0.9
nC_4	58.12	3.1	1.7	2.8	2.0
iC_5	72.15	2.1	1.4	1.7	1.6
nC_5	72.15	3.3	2.3	2.8	2.5
C_6	84.00	3.6	2.9	2.6	2.8
C_7	96.00	3.9	3.5	2.8	3.4
C_8	107.00	3.6	3.6	2.5	3.4
C_9	121.00	3.3	3.8	2.3	3.5
C_{10}	134.00	3.1	3.9	2.1	3.6
C_{11}	147.00	2.0	2.8	1.4	2.5
C_{12}	161.00	1.9	2.8	1.3	2.6
C_{13}	175.00	1.7	2.8	1.2	2.6
C_{14+}	311.95	19.7	58.1	13.4	52.7

(3) The density of the mix of solid pyrobitumen and pyrobitumen predecessor is a constant value during oil cracking;
(4) The oil cracking process is not affected by the internal pressure of the oil inclusion;
(5) The mutual solubility between the liquid oil and insoluble products (pyrobitumen and pyrobitumen predecessor) (Behar et al., 1992) during oil cracking can be neglected;
(6) The solid pyrobitumen and pyrobitumen predecessor does not affect the PVT phase behavior of the liquid oil. In order to simplify, the pyrobitumen and pyrobitumen predecessor are grouped together as "pyrobitumen" in the following sections.

4.2.2. Initial compositions in oil inclusions

Because oil cracking occurs over geological time scales, the initial components of oil cracking can be constrained by fluid inclusion measurement results. To compare the effects of oil cracking on oil inclusions with inferred different maturities, a yellow fluorescing low-maturity oil inclusion (oil inclusion A) from well F8 (3943 m) and a blue-white fluorescing high-maturity oil inclusion (oil inclusion B) from well FS1 (4321.7 m) were selected for composition modeling with an α-β composition model (Thiéry et al., 2002). This α-β composition modeling only requires the T_{ho} and F_{vo} of an oil inclusion, but a third parameter, usually the C_1 molar content, should be used to constrain the only α-β composition. In this study the C_1 molar content was obtained using the petroleum type determination method (Ping et al., 2012). Oil inclusion A homogenizes at 47.5 °C and has an F_{vo} of 3.1% at 20 °C, whereas oil inclusion B homogenizes at 128.6 °C and has an F_{vo} of 16.9% at 20 °C. Then, the α-β curves of these two inclusions were calculated (Thiéry et al., 2002), and values of $\alpha = 0.92$ and $\beta = 0.47$ were chosen for oil inclusion A and $\alpha = 0.92$ and $\beta = 0.59$ for oil inclusion B. The modelled detailed oil composition (mole percent and weight percent) according to the calculated α and β values (Thiéry et al., 2002) are shown in Table 2, and were used as the initial components of oil cracking in this study.

4.2.3. Procedure

The entire calculation process is divided into the following three steps.

First, the kinetic modeling of oil cracking requires a grouped composition (Table 1), so the single carbon number component in Table 2 needs to be combined into the twelve component types in accordance with the oil cracking composition model. The results are listed in Table 3, among which the content of saturated hydrocarbons, aromatic hydrocarbons, NSO fraction in $C_{6\text{-}13}$ and C_{14+} fractions were calculated based on mass conservation and the average mass ratio of saturated hydrocarbons to aromatic hydrocarbons (2.5) and saturated hydrocarbons to the NSO fraction (2.3) of reservoir oils in the northern Dongying Depression. Table 4 lists the critical parameters of all the components that are used to calculate the P-T phase diagram and isochore line with the equation of state (Hantschel and Kauerauf, 2009).

Second, these data were integrated with the thermal evolutionary history of the reservoir after the oils were trapped as oil inclusion A and oil inclusion B. Two different thermal evolution and burial histories from 4500 m in well FS1 and from 5755 m in well FS2 were chosen to constrain the oil cracking process to consider the influence of different thermal stress conditions on oil cracking (Fig. 7). The thermal histories were calibrated by using present-day formation temperature and vitrinite reflectance data. Crude oil cracking kinetic modeling (see Section 3.2 for details) was used to calculate changes in the components of the oil inclusions with changing time and reservoir temperature, obtaining the weight and mole percent of all the components in the oil inclusions during oil cracking.

Third, the internal pressure of oil inclusion A and oil inclusion B was calculated at all stages during oil cracking (Appendix A), according to the obtained molar contents of all the components. Then, the isochore and P-T phase diagrams were calculated using the new internal pressure of oil inclusion A and oil inclusion B after oil cracking (see Section 3.3 for details). Finally, the revised T_{ho}, F_{vo} and P_t by oil cracking were obtained. In order to assess the influence of P_t on the internal pressure of the oil inclusion during oil cracking, the initial trapping pressure values of the oil inclusions were artificially assigned to varying pressure conditions from hydrostatic pressure to overpressure. The initial trapping pressure, trapping depth and trapping time parameters are listed in Table 5.

Although the oil cracking scheme used in this study is independent of kerogen type (Vandenbroucke et al., 1999), the Es_4^L source rocks in the northern Dongying Depression mainly contain type I and type II organic matter (Cai, 2007; Wang, 2009; Yang et al., 2007). Thus the oils in the DBRs in the northern Dongying have a different character from oils generated from type I organic matter, which contain more aliphatic hydrocarbons, and fewer aromatic hydrocarbons than oils derived from type II/III kerogen (Tissot and Welte, 1984). These differences result in thermal cracking of oil derived from type I kerogen to occur at a higher temperature compared with that of oil derived from type II/III kerogen, or a mix

Table 3
The compositional contents of the grouped oil components for two oil inclusions from Table 2.

Composition	Oil inclusion A			Oil inclusion B		
	Molar percentage (mol %)	Molecular weight (g/mol)	Weight percentage (wt.%)	Molar percentage (mol %)	Molecular weight (g/mol)	Weight percentage (wt.%)
CO_2	0	44.0	0	0	44.0	0
C_1	34.7	16.0	5.2	47.9	16.0	9.6
C_2	6.5	30.1	1.8	7.9	30.1	3.0
$C_{3\text{-}5}$	16.0	57.5	8.7	14.5	56.6	10.3
$C_{6\text{-}13}$ SAT	16.3	121.0	18.7	11.4	121.0	17.4
$C_{6\text{-}13}$ ARO	6.7	117.8	7.5	4.8	115.7	7.0
C_{14+} SAT	11.2	299.2	31.7	7.6	299.2	28.8
C_{14+} ARO C	0	0	0	0	0	0
C_{14+} ARO U	4.5	299.2	12.7	3.1	299.2	11.5
C_{14+} NSO	4.0	362.2	13.7	2.7	362.2	12.4
Precoke	0	0	0	0	0	0
Coke	0	0	0	0	0	0

Table 4
Critical parameters of the oil components in Table 3 for the oil inclusion P-T calculation (Hantschel and Kauerauf, 2009).

Composition	Critical temperature/T_c (K)	Critical pressure/P_c (MPa)	Acentric factor/ω
CO_2	304.19	7.382	0.2276
C_1	190.56	4.599	0.0115
C_2	305.32	4.872	0.0995
$C_{3\text{-}5}$	430.72	3.599	0.2008
$C_{6\text{-}13}$ SAT	587.96	2.518	0.4003
$C_{6\text{-}13}$ ARO	618.13	3.703	0.3077
C_{14+} SAT	813.82	1.442	0.7797
C_{14+} ARO	813.82	1.442	0.7797
C_{14+} NSO	810.40	1.009	1.0190

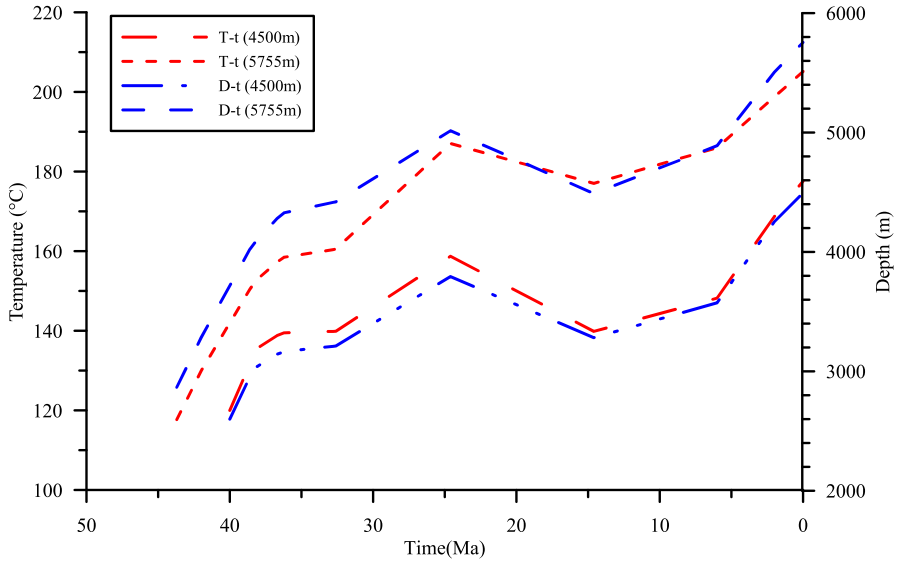

Fig. 7. The modelled thermal and burial history of present-day depths in 4500 m (well FS1) and 5755 m (well FS2) using 1D basin modeling (IES PetroMod 1D v11 software) in the Dongying Depression, Bohai Bay Basin, which were calibrated by present formation temperatures and vitrinite reflectance (R_o). T-t means formation temperature (left y axis) evolved with time, and D-t means burial depth (right y axis) evolved with time.

Table 5
Assumed initial trapping conditions of two oil inclusions in Table 2. Two trapping pressure ($P_{ci} = 1$ and $P_{ci} = 1.25$) were assigned to oil inclusions trapped at 2867 m and 117.7 °C with the thermal-burial history of present-day depth at 5755 m.

Present-day burial depth (D_p) (m)	Trapping temperature (T_t) (°C)	Trapping time (T_{tm}) (Ma)	Trapping depth (D_t) (m)	Pressure coefficient of initial trapping pressure ($P_{ci} = 1.00$)	Pressure coefficient of initial trapping pressure ($P_{ci} = 1.25$)	Pressure coefficient of initial trapping pressure ($P_{ci} = 1.50$)
				Initial trapping pressure (P_{ti}) (MPa)		
4500	120.0	40.0	2600	26.78	33.48	40.17
5755	117.7	43.7	2867	29.53	36.91	–

of type I and type II kerogen, because the C_{14+} saturates are the most stable group (Behar et al., 2008). Therefore, the modelled results in this study are more applicable to crude oils whose source rocks contain type I and type II organic matter.

4.3. Compositional changes and their effect on the fluorescence color of oil inclusions during oil cracking

Fig. 8 shows that the C_{14+} NSO in the two types of crude oil (Table 2) has the least stability and cracked first under both thermal evolutionary history conditions (Fig. 7). When the C_{14+} NSO component begins to crack during the initial stage of oil cracking, the other components increase correspondingly, which indicates that the pyrolysis products of the C_{14+} NSO component are mainly saturated hydrocarbons, aromatic hydrocarbons, pyrobitumen and gas hydrocarbons (Behar et al., 1992; Horsfield et al., 1992). Then, the C_{14+} ARO component begins to crack, because the thermal stability of the C_{14+} SAT component is higher than that of the C_{14+} ARO component under geological conditions. Under low thermal stress conditions (<180 °C) the main component of the C_{14+} fraction is the C_{14+} SAT component, and the oil is deficient in the C_{14+} NSO and C_{14+} ARO components. The ratio of saturated to aromatic hydrocarbons gradually increases with increasing thermal stress. This variation in the oil components with varying thermal stress is consistent with the results of previous studies (Behar et al., 2008; McNeil and BeMent, 1996; Vandenbroucke et al., 1999).

Hydrocarbons from the C_{14+} SAT, C_{6-13} SAT, C_{6-13} ARO and C_{3-5} components crack as the thermal stress continues to increase (>180 °C). Additionally, solid pyrobitumen forms under lower thermal stress (>140 °C) (Fig. 8) and continues to increase, which is consistent with oil cracking experiments (Hill et al., 2003). Therefore, when the T_f increases to 180 °C (at approximate 27 Ma, see Fig. 8C and D), the main cracking components of crude oil are from the C_{14+} fraction. For example, the C_{14+} NSO components decrease gradually and then disappear, forming a certain amount of pyrobitumen that is insoluble in organic components. As the T_f increases from 180 °C to 210 °C, both the C_{14+} and the C_{3-5} components begin to crack, forming large amounts of solid pyrobitumen and gaseous hydrocarbons as the C_{1-5} component, and the main liquid hydrocarbons are in the C_{6-13} ARO component. In addition, oil inclusion A cracks more quickly than oil inclusion B, because of the higher amount of heavy components (Fig. 8).

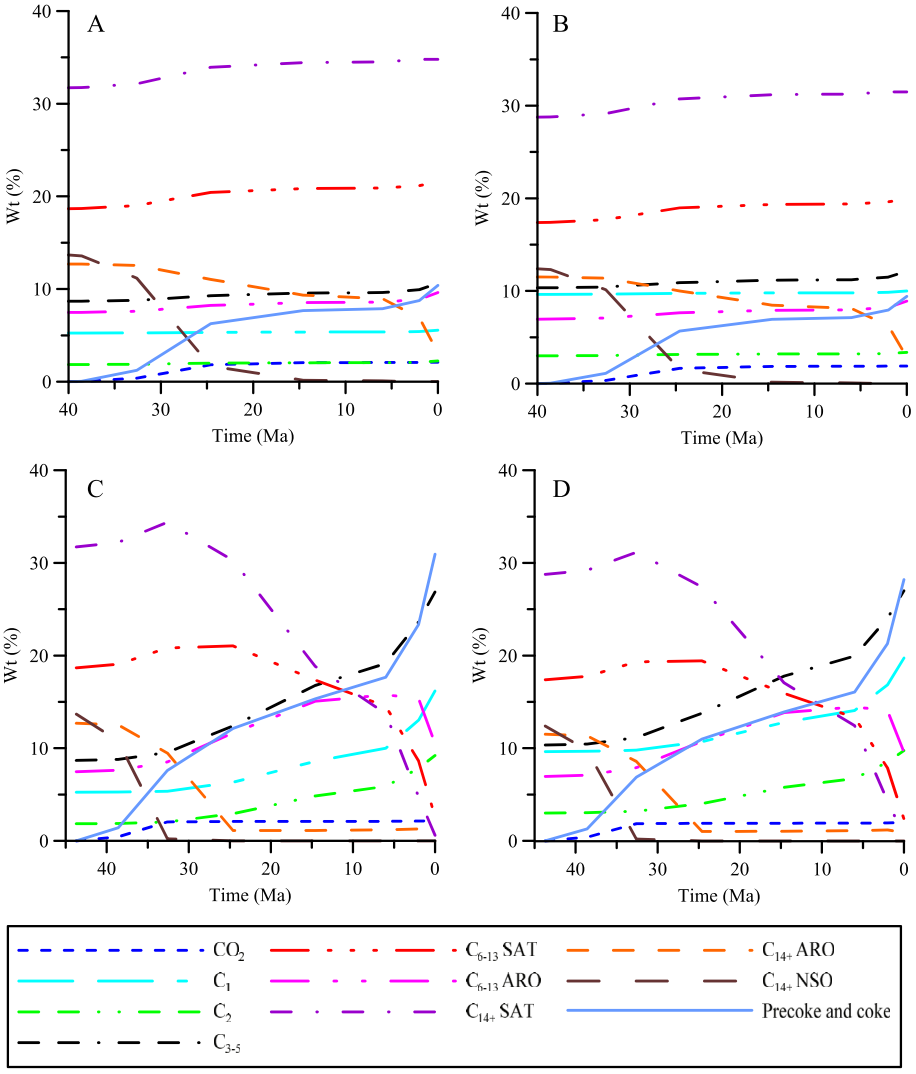

Fig. 8. The compositional variation of oil inclusion A and oil inclusion B in Table 1 with the two different burial histories from Fig. 7 during oil cracking. The compositional variation of (A) oil inclusion A and (B) oil inclusion B are shown for the thermal-burial history of present-day depth at 4500 m, while the compositional variation of (C) oil inclusion A and (D) oil inclusion B are shown for the thermal-burial history of present-day depth at 5755 m.

As oil cracking results in a decrease of C_{14+} NSO components and variation in the relative proportion of saturate and aromatic hydrocarbons, the fluorescence color of oil inclusion could change during oil cracking. Crude oils exhibit fluorescence under excitation by ultraviolet light, which results from the radiation of polycyclic aromatic hydrocarbons and heterocyclic hydrocarbons (Riecker, 1962). Because heterocyclic hydrocarbons exhibit weak red fluorescence, the fluorescence colors of crude oils are largely governed by the thermal evolution degree of polycyclic aromatic hydrocarbon components and the relative proportion of saturate to aromatic hydrocarbons in oil (Khorasani, 1987). Visible fluorescence from excitation by ultraviolet light is mainly produced by polycyclic aromatic hydrocarbons, which are the main components of C_{14+} ARO. The mass ratio of saturated to aromatic hydrocarbons ($K_{SAT/ARO}$) is redefined to understand changes in fluorescence color during oil cracking:

$$K_{SAT/ARO} = \frac{C_{6-14}\ SAT + C_{14+}\ SAT}{C_{14+}\ ARO} \quad (2)$$

A higher value of $K_{SAT/ARO}$ indicates that the content of C_{14+} ARO components is relatively low; thus, the oil inclusion fluorescence color shifts towards shorter wavelengths (blue shift). A lower value of $K_{SAT/ARO}$ indicates that the content of C_{14+} ARO components is relatively high; thus, the oil inclusion fluorescence color shifts towards longer wavelengths (red shift). Moreover, the oil conversion rate (T_r) is defined to illustrate the degree of oil cracking. T_r is expressed as:

$$T_r = \frac{MI_{C6+} - MR_{C6+}}{MI_{C6+}} \quad (3)$$

In Eq. (3), MR_{C6+} is the remaining mass of liquid C_{6+} fraction during oil cracking, and MI_{C6+} is the initial mass of liquid C_{6+} before oil cracking. According to Eq. (2) and Eq. (3), the fluorescence color changes with degree of oil cracking can be deduced based on changes in the relative contents of saturated and aromatic hydrocarbons during oil cracking.

Fig. 9 shows the relationship between T_r and $K_{SAT/ARO}$ for inclusion A and inclusion B (Table 2) under different trapping conditions (Table 5) and different thermal evolutionary histories (Fig. 7) during oil cracking. According to Fig. 9, the $K_{SAT/ARO}$ of the oil inclusions displays changes during three stages of oil cracking. First, when T_r is less than 13% and the corresponding T_f is lower than 160 °C, the $K_{SAT/ARO}$ value increases slightly compared to the initial value when trapped, which suggests that the relative content of C_{14+} ARO components in crude oil decreases slightly and that oil cracking has little influence on the fluorescence color during this stage of oil cracking. When T_r increases from 13% to 24% as the formation temperature increases from 160 °C to 190 °C, the $K_{SAT/ARO}$ value quickly increases from 6 to 46 because of the cracking of a large number of C_{14+} ARO components. The relative content of C_{14+} ARO decreases quickly and the fluorescence color shifts towards shorter wavelengths (blue shift) during this stage. Blue fluorescence of inclusions is expected to be achieved due to a very high $K_{SAT/ARO}$ value around 190 °C. At the same time, the aromatic hydrocarbons are diluted by saturated hydrocarbons, so the fluorescence intensity increases accordingly because of the reduction of the concentration quenching effect (Bertrand et al., 1986; Khorasani, 1987).

Afterwards, components with higher thermal stability such as $C_{6\text{-}14}$ ARO and $C_{6\text{-}14}$ SAT begin to crack, and their cracking products are low-carbon-number hydrocarbons and some C_{14+} ARO hydrocarbons. The C_{14+} SAT fractions crack more quickly during this stage, and the $K_{SAT/ARO}$ value begins to gradually decrease, even becoming lower than the initial trapping value at extreme oil cracking conditions (Fig. 9). The decrease of $K_{SAT/ARO}$ value at higher thermal stress is in accordance with the results of Behar et al. (2008) (see Figs. 9 and 10 therein). Please note that this does not contradict what happens in natural oils, which will be more and more depleted in both C_{14+} aromatics and NSOs with increasing maturity, because the absolute content of these in the modelled oil decreases continuously during the whole oil cracking process (Fig. 8).

Whether the fluorescence color of crude oil shifts towards longer or shorter wavelengths depends not only on the relative content of saturated and aromatic hydrocarbons, but also on the maturity of the aromatic hydrocarbons. For example, there is a strong blue shift of the spectrum of simple aromatic structures compared with those of complex aromatic assemblages (Khorasani, 1987). The C_{14+} ARO fraction becomes richer in simple aromatic structures with increasing thermal stress (T_r > 24%, T_f > 190 °C), accompanied by a decrease in the relative content of saturated and aromatic hydrocarbons. However, it is complicated to interpret the variation of fluorescence colors under such conditions. Simple aromatic structures are considered to be the main control on the variation of fluorescence color at this stage (Khorasani, 1987). Although the relative content of saturated and aromatic hydrocarbons decreases, the absolute content of aromatic hydrocarbons

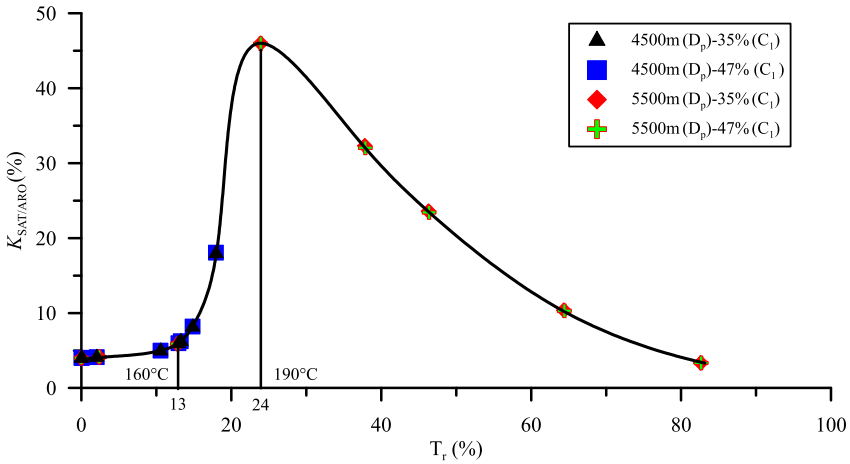

Fig. 9. The relationship between the transformation rate (T_r) during oil cracking and the ratio of saturated hydrocarbon to aromatic hydrocarbons ($K_{SAT/ARO}$). The present day burial depth (D_p) represents the thermal history that oil inclusions experienced after trapping, and C_1 represents the molar percent of methane in oil inclusions A and B.

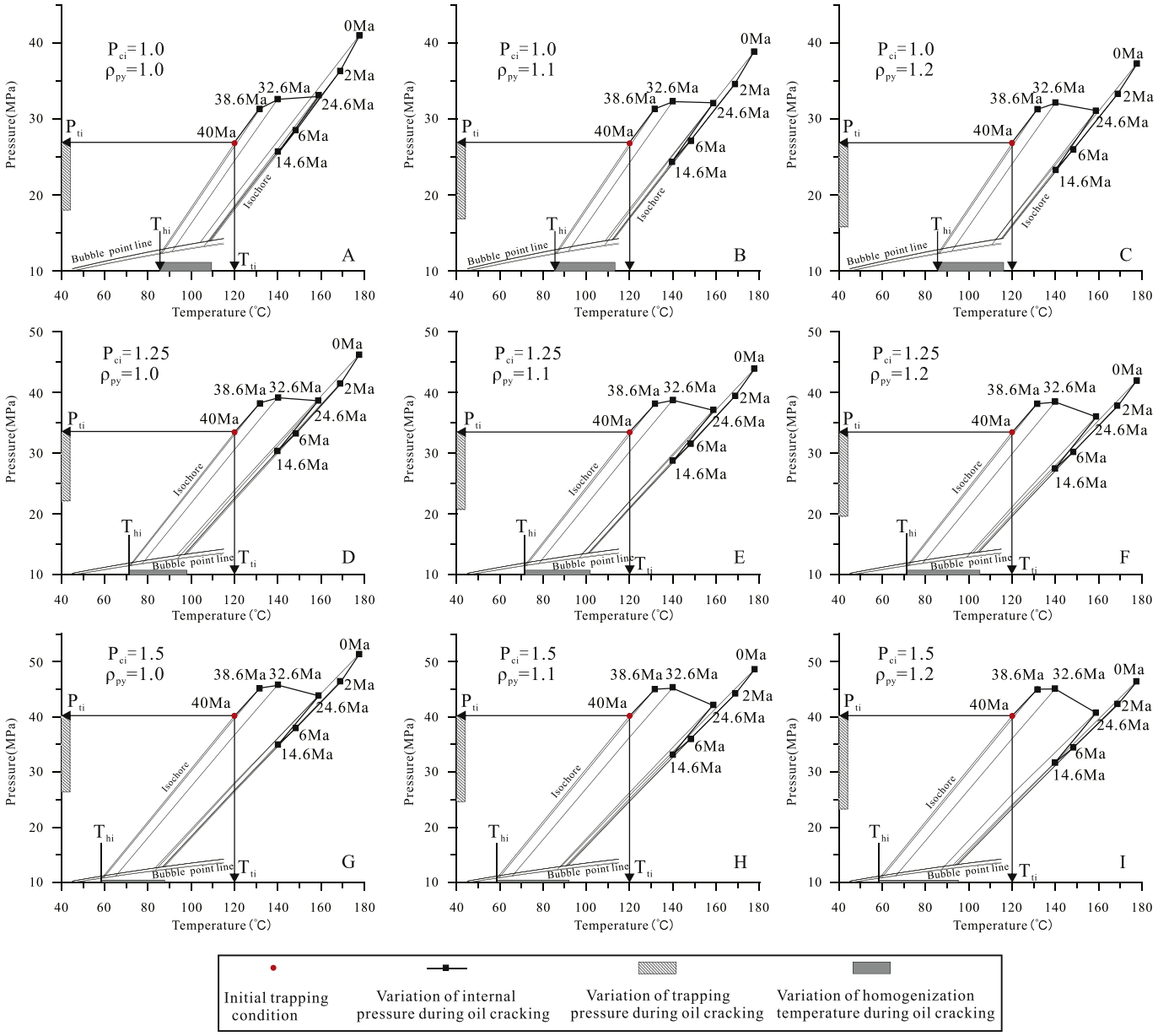

Fig. 10. The T_h and internal pressure (P_{in}) variations for oil inclusion A (Table 2) with the thermal-burial history of present-day depth at 4500 m (Fig. 7) under three different pressure coefficients of the initial trapping pressure (P_{ci}) conditions (1.0; 1.25; 1.5; Table 5) and three different pyrobitumen densities (ρ_{py}) (1.0 g/cm^3, 1.1 g/cm^3 and 1.2 g/cm^3). T_{hi}, T_{ti} and P_{ti} are the initial homogenization temperature, trapping temperature, and trapping pressure of oil inclusions, respectively.

decreases too. Therefore, the fluorescence color could show no obvious variation, or could continue to shift towards the blue color in this stage, depending on the fluorescence color when the oil reaches the highest $K_{SAT/ARO}$ value during oil cracking (approximately T_r = 24%). Nevertheless, the fluorescence intensity will decrease because of the decrease of the $K_{SAT/ARO}$ values. During the decrease of the $K_{SAT/ARO}$ and the content of C_{14+} ARO components, the fluorescence color will gradually change and even disappear as both the $C_{6\text{-}14}$ ARO and C_{14+} ARO components completely crack.

In summary, the oil inclusion fluorescence color and intensity are hardly affected during the initial stages of oil cracking (T_r < 13%, T_f < 160 °C). As the degree of oil cracking increases (13% < T_r < 24%, 160 °C < T_f < 190 °C), the oil inclusion fluorescence color shifts towards shorter wavelengths (blue color) and the fluorescence intensity increases. As oil cracking progresses (T_r > 24%, T_f > 190 °C), the fluorescence color may not observedly change, or may continue to shift towards the blue color, accompanied by a decrease of fluorescence intensity. The fluorescence color will gradually change and even disappear as both the $C_{6\text{-}14}$ ARO and C_{14+} ARO components completely crack.

The fluorescence spectra parameters of oil inclusions from wells in the northern Dongying Depression and other wells in the Dongying Depression (Fig. 5) show a concordant tendency, with the fluorescence varying according to the compositional modeling of oil cracking. Four types of oil inclusion maturities exist according to the λ_{max} values in Fig. 5A. The least mature oil inclusions have λ_{max} values from 570 nm to 595 nm and the most mature oil inclusions have λ_{max} values from 440 nm to 450 nm, while most of the oil inclusions have λ_{max} values from 480 nm to 550 nm. The least mature oil inclusions were only detected shallower than 3100 m and are thought to contain more polycyclic aromatic hydrocarbons and C_{14+} NSO components. Oil inclusions with λ_{max} from 530 nm to

549 nm are the most abundant of the four types of oil inclusions, and are believed to have been generated from a mature source rock in the oil window. This type of oil inclusion is thought to have higher maturity and is distributed at depths from 1500 m to 4000 m. Only oil inclusions with λ_{max} less than 500 nm can be found deeper than 4000 m; it is thought that these have more saturated hydrocarbons than polycyclic aromatic hydrocarbons. Generally, the maturity of oil inclusions as inferred from fluorescence spectroscopy increases with burial depth (Fig. 5).

Oil inclusions represent paleo-petroleum fluids that were trapped during oil charging, so the absence of mature oil inclusions (530 nm < λ_{max} < 549 nm) below 4000 m cannot be interpreted to be due to a lack of oil charging during the generation of mature oil. Interestingly, the present-day T_f is approximately 160 °C at 4000 m in the northern Dongying Depression (Fig. 2B), which is in accordance with the initial temperature (160 °C) for a rapidly increasing $K_{SAT/ARO}$ from oil cracking kinetic modeling (Fig. 9). The rapid cracking of C_{14+} ARO components is interpreted to indicate a shift in the λ_{max} values of the oil inclusions from 530 to 550 nm to less than 500 nm when the present-day depth exceeded 4000 m with a T_f over 160 °C (Fig. 5A). In addition, the λ_{max} values from 530 nm to 549 nm do not change shallower than 4000 m, but their corresponding $Q_{(650/500)}$ and QF-535 values gradually decrease with increasing depth (Fig. 5B and C). The most likely reason is the cracking of C_{14+} NSO components at low thermal stress, for which there is evidence from the results of compositional modeling during oil cracking (Fig. 8). On the other hand, the λ_{max} values of the fluorescence spectra parameters are not sensitive to low thermal stress (<160 °C) compared to $Q_{(650/500)}$ and QF-535, which are easily modified by variations in the C_{14+} NSO content. Consequently, it is better to distinguish multiple episodes of oil charging using the λ_{max} parameter rather than $Q_{(650/500)}$ and QF-535 parameters when analyzing the characteristics of the fluorescence spectra of oil inclusions.

4.4. Factors that control the effect of oil cracking on the T_{ho}

Once the oil inclusion components are established, T_{ho} can be determined by combining the formation temperature and internal pressure of the oil inclusion using the equation of state. T_{ho} greatly depends on the internal pressure of the oil inclusion (Ping and Chen, 2011). However, the internal pressure of an oil inclusion is controlled by changes in oil composition during oil cracking, and on the volume increase of solid pyrobitumen, which simultaneously leads to a volume decrease of the liquid phase oil in the oil inclusion. The volume of solid pyrobitumen depends on its generated amount and its density. Generally speaking, the density of pyrobitumen (ρ_{py}) increases with increasing thermal maturity and ranges from 1.0 g/cm^3 to 1.2 g/cm^3 (Jacob, 1989). Published data regarding changes in ρ_{py} with thermal maturity are lacking, so this study sets ρ_{py} as a variable that influences the internal pressure of the oil inclusion during oil cracking, and the densities of 1.0 g/cm^3, 1.1 g/cm^3 and 1.2 g/cm^3 were used to calculate the internal pressure and T_{ho} during oil cracking.

Fig. 10 shows the changes in T_{ho} and the internal pressure of oil inclusion A with increasing degree of oil cracking for various pressure coefficients of initial trapping pressure and pyrobitumen density conditions. Oil inclusion A was initially trapped at 120 °C under different trapping pressure (Table 5) and various ρ_{py}. The thermal-burial history of oil inclusion A was the same as that at the present-day burial depth of 4500 m, as shown in Fig. 7. According to Fig. 10, both trapping pressure and ρ_{py} have significant influence on T_{ho} during oil cracking; more importantly, the various trends of T_{ho} from Fig. 10 are not consistent with the results of Okubo (2005), who concluded that T_{ho} continuously decreases during oil cracking. However, our results show that the T_{ho} increases as oil cracking progresses, with the maximum change in T_{ho} being close to 40 °C (Fig. 10I). In addition, the higher the trapping pressure, the greater the influence of oil cracking on T_{ho}. For example, when the pressure coefficient of the initial P_t increases from 1.0 to 1.5, T_{ho} vap 10 A, D, and G). The higher the ρ_{py} value, the greater the influence of oil cracking on T_{ho}. For example, if ρ_{py} increases from 1.0 to 1.2, T_{ho} variation increases from 30 °C to 40 °C under the same pressure coefficient of the initial P_t (Fig. 10G, H, and I).

Fig. 11 illustrates how oil cracking influences the T_{ho} value of the more mature oil inclusion B after it was trapped. The variation in T_{ho} ranges from 10 °C to 20 °C during oil cracking at different initial P_t and ρ_{py} (Fig. 11A and I). Although the initial P_t and ρ_{py} have the same influence on the changes in T_{ho} as for the less mature oil inclusion A during oil cracking, the effect of oil cracking on T_{ho} of oil inclusion B is less than that for oil inclusion A. Thus, the higher the maturity of the crude oil in the oil inclusion, the smaller the influence of oil cracking on T_{ho}.

The reason why oil cracking increases T_{ho} is that C_{14+} NSO and C_{14+} ARO hydrocarbons are the main components that undergo thermal breakdown during initial oil cracking (Fig. 8A), and few gas hydrocarbons are generated during this process. The solid pyrobitumen that progressively forms in these oil inclusions both consumes the mass of liquid hydrocarbons and reduces the volume that the liquid hydrocarbons occupy. However, the density of pyrobitumen is much higher than that of liquid hydrocarbons, so the deceasing rate of the mass of liquid hydrocarbons is higher than that of the volume of liquid hydrocarbons. Thus, the density of the liquid oil decreases and the isochores of the oil inclusions in Figs. 10 and 11 shift to the right in the P-T phase diagram, which finally leads to an increase in T_{ho} as oil cracking progresses. Although changes in the oil components have little influence on the P-T phase diagram (the bubble point lines nearly coincide in Figs. 10 and 11) during low-degree oil cracking (usually T_f < 180 °C), they have great influence on changes in the isochores of oil inclusions and thus affect T_{ho}. Okubo (2005) showed that the T_{ho} values (73 °C-33 °C) in the Shin-Kumoide SK-1D well at a depth of 4040–4810 m decrease constantly with increasing depth, but proposed that this could not be caused by oil cracking, but instead reflected the paleo-trapping pressure characteristics (Ping and Chen, 2011). The formation temperature at a depth of 4040–4810 m ranges from 135 °C to 165 °C in the Shin-Kumoide SK-1D well, so oil cracking should increase T_{ho} during oil cracking according to the current study.

Oil cracking in oil inclusions must have occurred during the geologic past, as shown by the presence of solid bitumen in the oil inclusions from below 3900 m in the northern Dongying Depression (Fig. 4). However, a decreasing trend of T_{ho} as observed by Okubo (2005) was not seen, despite measuring over 900 T_{ho} values from 3500 to 4300 m in the northern Dongying Depression (Fig. 6). Rather two types of variation in T_{ho} were observed. The first trend is that the ranges of T_{ho} exhibit no obvious changes in deeper reservoirs compared to shallow reservoirs, such as the T_{ho} values from the Shengtuo area (Fig. 6A–C). Fig. 6B shows that the T_{ho} values for yellow fluorescing oil inclusions from 3951.8 to 3952.9 m are much higher than those of both yellow fluorescing and blue-white fluorescing oil inclusions from 3672 m (Fig. 6A and B). This result is attributed to oil cracking because: 1) yellow fluorescing oil inclusions are easier to crack compared to blue-white fluorescent oil inclusions; 2) yellow fluorescing oil inclusions may be trapped earlier than blue-white fluorescing oil inclusions, which could result in longer heating; and (3) solid bitumen was detected in the oil inclusions (Fig. 4b-c).

However, the T_{ho} range of the blue-white fluorescing oil inclusions from 4358.49 m in well T765 (Fig. 6C) did not change compared to the T_{ho} range of those from 3951.8 to 3952.9 m in well

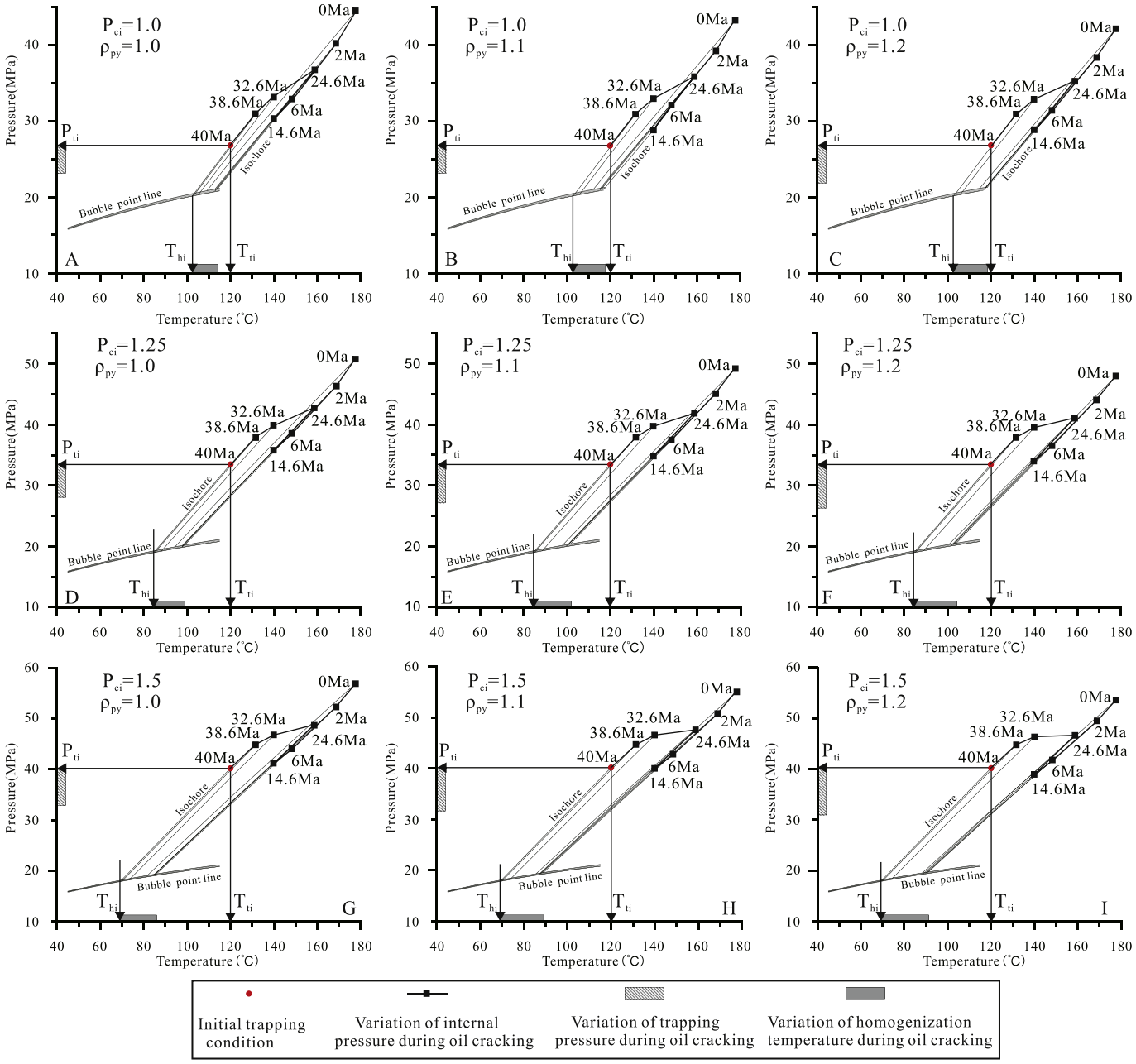

Fig. 11. The T_h and internal pressure (P_{in}) variations for oil inclusion B (Table 2) with the thermal-burial history of present-day depth at 4500 m (Fig. 7) under three different pressure coefficients of the initial trapping pressure (P_{ci}) conditions (1.0; 1.25; 1.5; Table 5) and three different pyrobitumen densities (ρ_{py}) (1.0 g/cm^3, 1.1 g/cm^3 and 1.2 g/cm^3). T_{hi}, T_{ti} and P_{ti} are the initial homogenization temperature, trapping temperature, and trapping pressure of oil inclusions, respectively.

T765 (Fig. 6B). The T_{ho} distributions in the Shengtuo area seem not to agree with the modelled results in this study. However, in consideration of the present-day formation pressure below 3900 m in the Shengtuo area and the absence of solid bitumen in the oil inclusions from 4358.49 m in well T765, overpressure could have played an important role in preventing oil cracking in the blue-white fluorescing oil inclusions from 4358.49 m in well 765, restricting T_{ho} to low values (Al Darouich et al., 2006; Chen et al., 2014; Snape et al., 2007). Fig. 2A shows that strong overpressure developed where the present-day pressure gradient at 4358.49 m in well T765 is nearly 20 MPa/km. In addition, the coeval aqueous inclusions and blue-white fluorescing oil inclusions have measured T_{ho} values between 150 °C and 160 °C, which suggests that blue-white fluorescing oil was recently trapped under overpressure conditions (Ping et al., 2017). Thus, high trapping pressure, recent trapping and higher-maturity oil may have led to a low-degree of oil cracking and, thus, the least modification of T_{ho}.

Oil inclusions were trapped within a calcite vein at 3943.0 m in well F8, and coeval aqueous inclusions have measured T_h values between 130 °C and 155 °C (Fig. 6D), which suggests that the oil inclusions were trapped within the last several million years (present-day T_f = 150 °C). Moreover, the T_{ha} values of coeval aqueous inclusions and the T_{ho} of oil inclusions from 4055.35 m to 4181.5–4201.5 m in well F8 are higher than those from 3943.0 m (Fig. 6E and F). Therefore, it is inferred that the oil inclusions from 4055.35 m to 4201.5 m in well F8 were trapped at the same time as those from 3943.0 m, or slightly later. Thus, the trapping pressure of oil inclusions from 4055.35 m to 4201.5 m was larger than the

trapping pressure of oil inclusions from 3943.0 m, with the largest difference reaching 6 MPa if a lithostatic pressure gradient is used to calculate increasing pressure over no greater than 300 m. In addition, the maturity of oil inclusions from 4055.35 m to 4201.5 m is lower than that from 3943.0 m according to the fluorescence spectra parameters in Fig. 5. Consequently, oil inclusions that were trapped from 4055.35 m to 4201.5 m should have a lower T_{ho} than the oil inclusions containing less mature oil from 3943.0 m according to the P-T phase diagram, because of the latter's slightly higher P-T gradient. However, Fig. 6E and F shows that the T_{ho} values from 4055.35 m to 4201.5 m are much larger than that from 3943.0 m (Fig. 6D). The best explanation could be the effects of oil cracking on the T_{ho} values of oil inclusions combined with the presence of solid bitumen in the oil inclusions (Fig. 4f′, g′, and h′) and the modelled results for T_{ho} during oil cracking. The T_{ho} values from 4321.7 to 4323.6 m in well FS1 (Fig. 6I) were much higher than those at shallower depths (Fig. 6G–H). The high formation temperature (T_f = 185 °C), the presence of pyrobitumen in intergranular pores (Fig. 4p) and solid bitumen in oil inclusions (Fig. 4j′-n′), except for blue fluorescing oil inclusions (Fig. 4o′), and the increasing T_{ho} from 3943 m to 4323.6 m all indicate the effects of oil cracking.

4.5. Variations in internal pressure and the predicted P_t in oil inclusions during oil cracking

The differences in the homogenization temperature between aqueous and oil inclusions (T_{ha}-T_{ho}) defined as ΔT_h, the F_{vo} and the degree of pyrobitumen filling in the oil inclusions (F_{vpy}) during oil cracking are used to further analyze and compare the influence of oil cracking on T_{ho} and the internal pressure. The difference between T_{ha} and T_t for aqueous inclusions is generally small in most petroliferous sedimentary basins (Hanor, 1980). Therefore, T_t was used as the T_{ha} value in this study (Munz et al., 2004; Thiéry, 2006; Tseng and Pottorf, 2002). ΔT_h can also represent the difference between T_t and T_{ho} (T_t–T_{ho}). F_{vo} is the volume percent of gas bubbles to gas- and liquid-phase hydrocarbons in oil inclusions at room temperature (20 °C), and F_{vpy} is the volume percent of solid pyrobitumen to the total fluid inclusion, including oil, gas and solid pyrobitumen. For simplicity, the intermediate value of the density range of pyrobitumen (1.0–1.2 g/cm^3) was selected (1.1 g/cm^3) as the input value to calculate the changes in T_{ho}, ΔT_h, F_{vo} and F_{vpy} in oil inclusions A and B (Table 2) at different initial trapping pressures (Table 5) and under different thermal evolutionary histories (Fig. 7). The results are presented in Figs. 12–15.

The initial homogenization temperatures of oil inclusions A and B (Table 2), which were trapped at a given trapping temperature, depend on their initial trapping pressure. The higher the initial trapping pressure value, the lower the initial homogenization temperature value and the higher the ΔT_h value (Figs. 12–15). Thus, T_{ho} and ΔT_h can be used to indicate whether the formation developed paleo-overpressure (Burruss, 2003; Ping and Chen, 2011; Pironon and Bourdet, 2008). During initial oil cracking (T_f < 180 °C) (Figs. 12 and 13), T_{ho} tends to increase on the whole, and the corresponding values of ΔT_h and the predicted P_t all decrease as oil cracking progresses regardless of the oil inclusion's components (inclusions A and B). The difference is that oil inclusion B, which has a higher maturity, will be less affected by oil cracking compared to oil inclusion A, which has a lower maturity (Figs. 12 and 13).

For inclusions with the same maturity, the influence of the oil cracking process on the trapping pressure differs greatly under different trapping pressures. When the initial P_t is higher, the influence of oil cracking on the predicted P_t is greater. For example, the reconstructed P_t for oil inclusion A decreases from 26.8 MPa before oil cracking to a minimum of 16.8 MPa during oil cracking when the pressure coefficient of the initial P_t is 1.0. A maximum deviation of 10 MPa from oil cracking is shown in Fig. 12B. If the pressure coefficient of the initial P_t is increased to 1.5, the deviation of the reconstructed P_t from oil cracking is nearly 16 MPa (Fig. 12H), with a relative error (the percentage of the deviation between the reconstructed P_t relative to the initial P_t) of approximately −40%. Fig. 13B, E, and H show the reconstructed P_t for oil inclusion B during oil cracking, whose deviations range from 3.3 MPa to 8.3 MPa with a relative error from −12% to −20%. The more mature the included oil, the more difficult modifying P_t through oil cracking process.

In addition, the internal pressure of the oil inclusion increases with increasing T_f in Fig. 12B, E, and H and Fig. 13B, E, and H. However, the internal pressure increases more slowly than the hydrostatic pressure, which suggests that reservoir oil cannot develop overpressure but can develop hydrostatic pressure or underpressure during a lower-degree of oil cracking (T_r < 24%, T_f < 190 °C), if the oil inclusion is considered as a reservoir that is full of crude oil. In fact, it is impossible for the open system of the reservoir to develop the same pressure as the closed system of oil inclusions during oil cracking, because of imperfect sealing of the reservoir. Therefore, the calculated internal pressure of oil inclusions is the maximum pressure that could be developed in the open system of the reservoir during oil cracking. This result contrasts with that of a previous study, which concluded that the lithostatic gradient is reached after approximately 1.0% of the oil is cracked (Barker, 1990). Several reasons may explain why the Barker (1990) results suggested that oil cracking generates ultra-high pressure after only 1.0% of the oil is cracked. Most importantly, the equation for the thermal cracking of oil into gas that was used by Barker (1990) was not appropriate at an initial oil cracking stage because it generated excessive gaseous hydrocarbons during this stage, and the initial and final temperatures (111 °C - 149 °C) for the cracking of oil to gas were too low. In fact, many laboratory experiments have demonstrated that primary C_2-C_5 hydrocarbon gas is generated during early oil cracking and that abundant C_1 gas is generated during the later stages of oil cracking (Behar et al., 1992; Hill et al., 2003; Tian Hui et al., 2006). Among gaseous hydrocarbons, the C_1 molar content in crude oil greatly affects the P-T phase behavior, e.g., the saturation pressure of crude oil (Ping et al., 2013).

F_{vo} is closely related to T_{ho} once the petroleum type is determined (Bourdet et al., 2008). Thus, F_{vo} should follow the variation trends of T_{ho} during oil cracking. Figs. 12–15 show that both F_{vo} and F_{vpy} increase throughout initial oil cracking, and any changes in F_{vo} and F_{vpy} also depend on initial P_t and the maturity of the oil in the oil inclusion. The greater the maturity and the higher the initial P_t value, the less that F_{vo} and F_{vpy} change.

Figs. 14 and 15 show the variations in T_{ho}, ΔT_h, internal pressure, the reconstructed P_t, F_{vo} and F_{vpy} under a high-degree of oil cracking (T_r < 83%, T_f < 205 °C). Unlike the continuous increase in T_{ho} during initial oil cracking, T_{ho} presents three different trends. (1) T_{ho} increases with ΔT_h and the reconstructed P_t decreases correspondingly until T_f increases to 160 °C; although the internal pressure of the oil inclusion tends to increase, its corresponding pressure coefficient tends to decrease. (2) When T_f increases from 160 °C to 190 °C, T_{ho} decreases gradually as the corresponding ΔT_h increases, and the reconstructed P_t begins to increase close to the initial P_t value. (3) T_f increases from 190 °C to 205 °C, which is the primary stage for the cracking of oil to gas. T_{ho} appears to decrease rapidly, even reaching negative values, while the internal pressure of the oil inclusion quickly increases close to or over the lithostatic pressure, and the reconstructed P_t is much higher than the initial P_t value when the oil inclusions were trapped, which is accompanied by a continuous increase in F_{vpy} and a quick decrease in F_{vo} to zero.

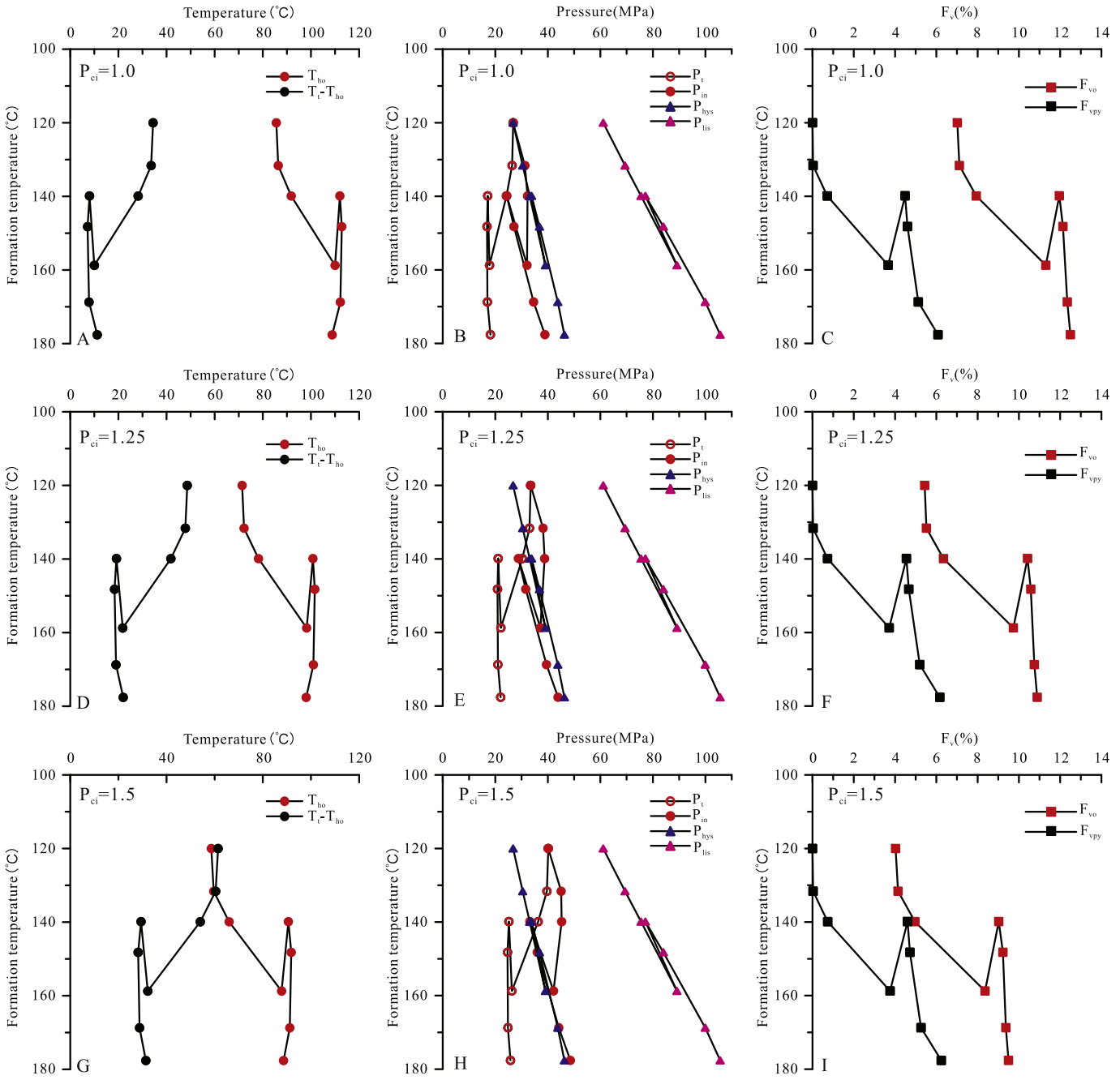

Fig. 12. Variation of oil inclusion A (Table 2) homogenization temperature (T_{ho}), internal pressure (P_{in}), bubble filling degree (F_{vo}) and volume percent of pyrobitumen (F_{vpy}) with the thermal-burial history of present-day depth at 4500 m (Fig. 7) under different pressure coefficients of the initial trapping pressure (P_{ci}) (Table 5). T_t: trapping pressure of oil inclusion; P_t: trapping pressure of oil inclusions; P_{hys}: hydrostatic pressure of the reservoir during oil cracking in an oil inclusion; $P_{lis:}$ lithostatic pressure of the reservoir during oil cracking in an oil inclusion.

Thus, the oil inclusions are single liquid phases at room temperature when there is a high degree of oil cracking. These results are consistent with the conclusion that the presence of single-phase liquid oil inclusions could be considered as a good indicator of high-pressure regimes (Pironon and Bourdet, 2008). The reason why T_{ho} decreases quickly under a high-degree of oil cracking (T_r > 24%, T_f > 190 °C) is that a quick increase in the internal pressure occurs because primary gas hydrocarbon generation shifts the slopes of the isochores of oil inclusions to a higher pressure, eventually reaching the bubble point curve at a low temperature.

The open system of a reservoir is quite different from the closed system in an oil inclusion where there is limited interaction between the hydrocarbon and rock, and the hydrocarbons remain stable to much higher temperatures than in systems open to interaction with rock (Giggenbach, 1997). Moreover, if the inhibition of overpressure on oil cracking is considered (Al Darouich et al., 2006; Chen et al., 2014; Snape et al., 2007), the initial temperature for the effect of oil cracking on T_{ho} and a sharp decrease in T_{ho} may be much higher than that in this study, where the inhibition of overpressure on oil cracking was not considered. In fact, the strong

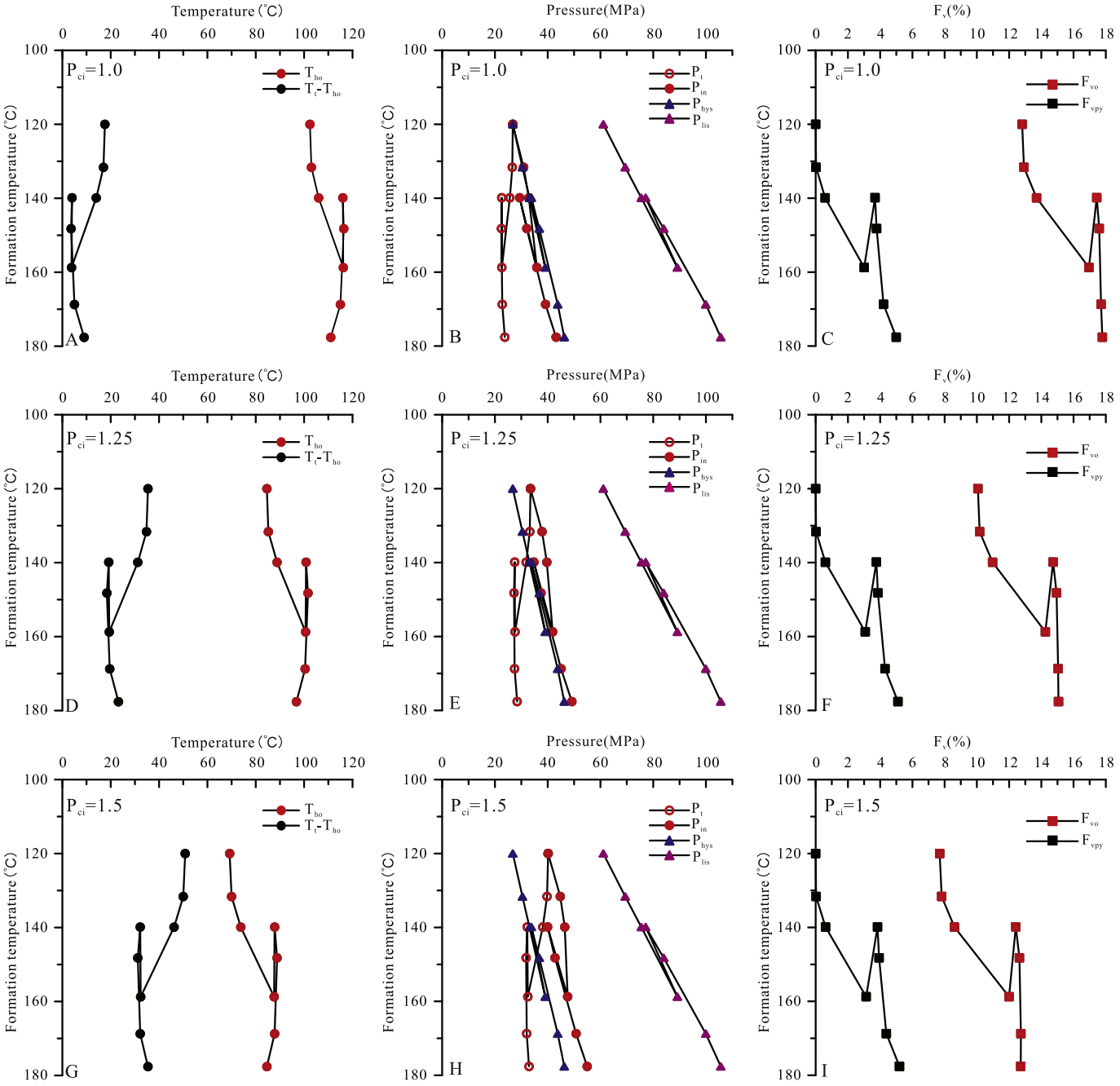

Fig. 13. Variation of oil inclusion B (Table 2) homogenization temperature (T_{ho}), internal pressure (P_{in}), bubble filling degree (F_{vo}) and volume percent of pyrobitumen (F_{vpy}) with the thermal-burial history of present-day depth at 4500 m (Fig. 7) under different pressure coefficients of the initial trapping pressure (P_{ci}) (Table 5). T_t: trapping pressure of oil inclusion; P_t: trapping pressure of oil inclusions; P_{hys}: hydrostatic pressure of the reservoir during oil cracking in an oil inclusion; $P_{lis:}$ lithostatic pressure of the reservoir during oil cracking in an oil inclusion.

overpressure (Fig. 2A), the absence of solid bitumen in oil inclusions (Fig. 4d′) and the low T_{ho} (Fig. 6C) at a depth of 4358.49 m in well T765 shows that oil cracking was restrained by overpressure to some extent. Therefore, it is concluded that oil inclusions that are trapped under overpressure conditions are more difficult to modify by oil cracking compared to those that are trapped under normal pressure systems. Thus T_{ho} could be usable for the reconstruction of oil and gas charging histories in much deeper reservoirs.

4.6. Recognizing the degree of crude oil cracking

The distribution of C_{6+} compositions strongly depends on the degree of oil cracking. Fig. 16 shows the relationship between the T_r and variations of T_{ho} (ΔT_{ho}) during crude oil cracking under different trapping conditions for oil inclusions A and B. As shown in Fig. 16, the T_{ho} variations are mainly controlled by the degree of crude oil cracking. When T_r is less than 13%, which corresponds to a T_f value of 160 °C, crude oil cracking increases the T_{ho} value. When T_r is greater than 13% (T_f > 160 °C), T_{ho} decreases as the degree of

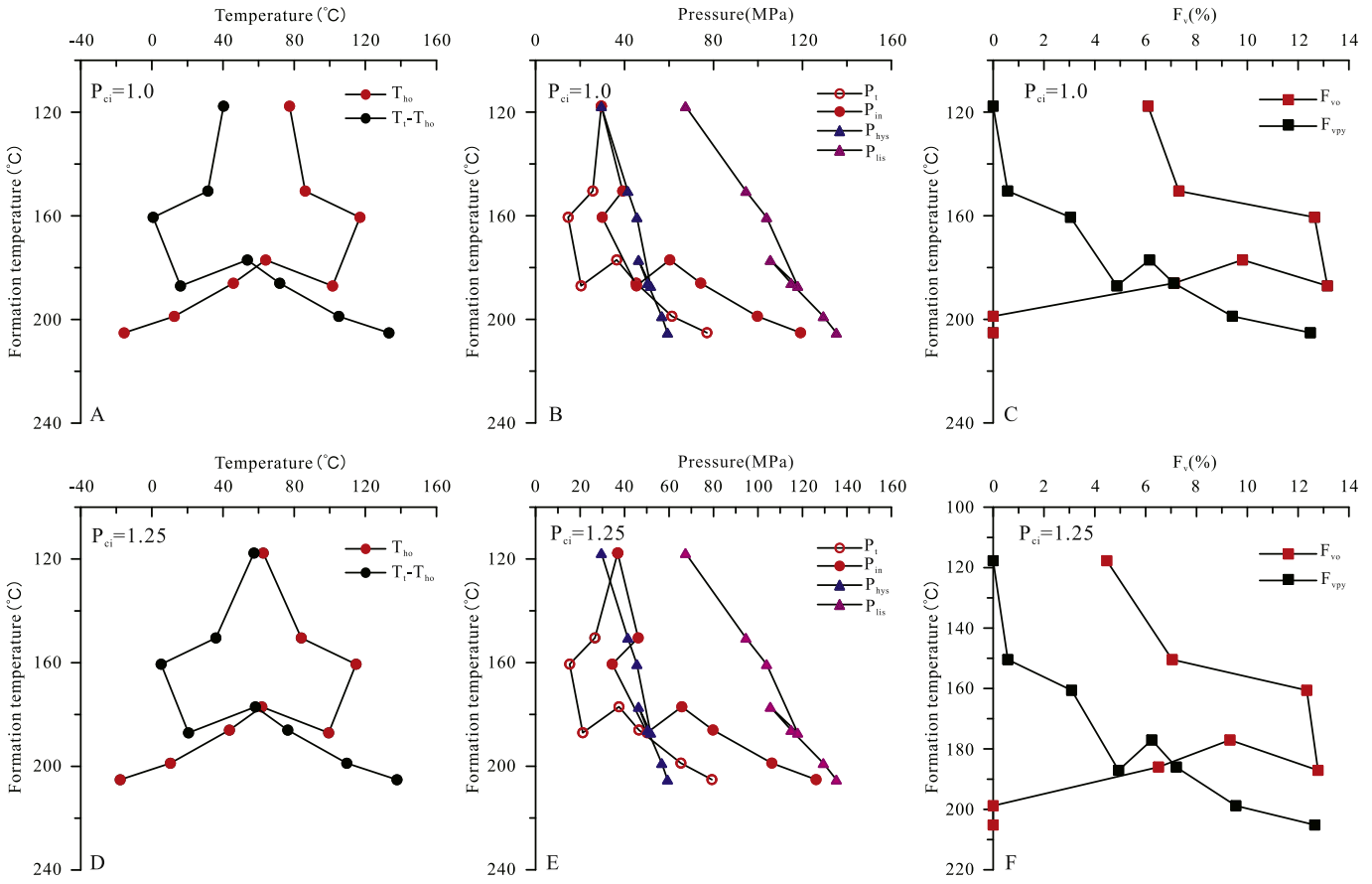

Fig. 14. Variation of oil inclusion A (Table 2) homogenization temperature (T_{ho}), internal pressure (P_{in}), bubble filling degree (F_{vo}) and volume percent of pyrobitumen (F_{vpy}) with the thermal-burial history of present-day depth at 5755 m (Fig. 7) under different pressure coefficients of the initial trapping pressure (P_{ci}) (Table 5). T_t: trapping pressure of oil inclusion; P_t: trapping pressure of oil inclusions; P_{hys}: hydrostatic pressure of the reservoir during oil cracking in an oil inclusion; P_{lis}: lithostatic pressure of the reservoir during oil cracking in an oil inclusion.

crude oil cracking increases. Although T_{ho} begins to decrease, generally this value is still higher than its initial homogenization temperature when T_r ranges from 13% to 24% (160 °C < T_f < 190 °C). When T_r is higher than 24% and lower than 38%, T_{ho} may be higher or lower than its initial homogenization temperature, which depends on its initial P_t and the initial oil compositions of the oil inclusions. The heavier the oil and the higher the initial P_t value, the larger the ΔT_{ho} variation when T_r is lower than 13%. When T_r reaches as high as 38%, stronger oil cracking is required to reduce T_{ho} to its initial homogenization temperature ($\Delta T_{ho} = 0$ °C) (Fig. 16).

As solid pyrobitumen is continuously generated during oil cracking, F_{vpy} constantly increases, and the value of F_{vpy} depends on the initial trapping components and the thermal evolutionary history of the oil inclusions, but has little relationship with its initial P_t value (Fig. 17). Generally, the F_{vpy} value of an oil inclusion has a positive correlation with T_r and thus can be used to indicate the degree of oil cracking in the oil inclusion. Once the T_r value of the oil inclusion is known according to F_{vpy} in Fig. 17, the approximate ΔT_{ho} from oil cracking can be estimated based on the correlation between T_r and ΔT_{ho} in Fig. 16. In addition, the degree of oil cracking in the oil inclusion can be evaluated qualitatively by comparing the pyrobitumen content and the fluorescence characteristics of the oil inclusion. For example, a low pyrobitumen content and strong fluorescence intensity in an oil inclusion suggests that oil cracking is at an initial stage (T_r < 13%). If the pyrobitumen content is high, the blue fluorescence intensity is weak or even no fluorescence, and no gas bubble is present (single-phase liquid oil inclusion), then the oil may have been significantly cracked (T_f > 200 °C, T_r > 64%, at least).

The presence of solid bitumen in oil inclusions is one of the lines of evidence to justify the oil cracking phenomenon. However, solid bitumen can form due to various other geological processes, e.g., natural gas injection (gas deasphalting), biodegradation, and water washing (Curiale, 1986), and these processes may explain solid bitumen where it is trapped together with crude oil in fluid inclusions in diagenetic minerals. The volume filling fraction of solid bitumen in the same fluid inclusion assemblage can vary greatly when the solid bitumen is generated prior to the trapping of oil inclusions, and oil inclusions that do not contain solid bitumen and those that contain varied amounts of solid bitumen can also be measured. The formation of solid bitumen generated during oil cracking is kinetically controlled (Behar et al., 2008), while the gas deasphalting process is controlled by the phase equilibria of reservoir fluids (Evans et al., 1971) and this precipitated bitumen mainly contains asphaltenes (Blanc and Connan, 1994), which are significantly different from the highly condensed bitumen (pyrobitumen) generated during oil cracking. Pyrobitumen that forms from oil cracking shows consistent F_{vpy} values in the same fluid inclusion assemblage (Fig. 4n′). In addition, the color of solid bitumen under transmitted and UV light can also be used to judge if the solid bitumen originates from oil cracking or from gas injection. Solid bitumen generated from oil cracking is black to dark brown under transmitted light and has no visible fluorescence color under UV light (Hunt, 1995), while solid bitumen from gas injection

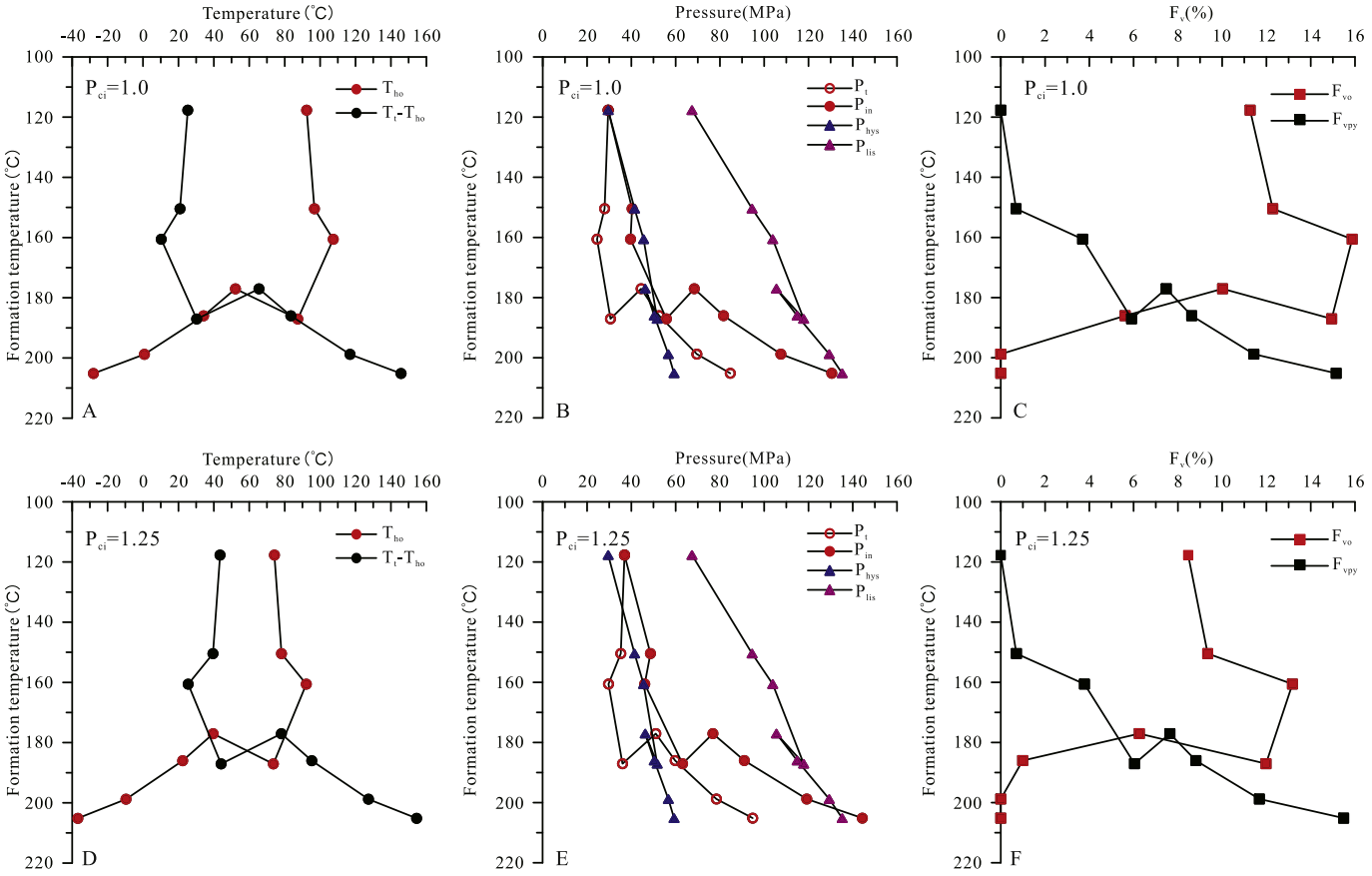

Fig. 15. Variation of oil inclusion B (Table 2) homogenization temperature (T_{ho}), internal pressure (P_{in}), bubble filling degree (F_{vo}) and volume percent of pyrobitumen (F_{vpy}) with the thermal-burial history of present-day depth at 5755 m (Fig. 7) under different pressure coefficients of the initial trapping pressure (P_{ci}) (Table 5). T_t: trapping pressure of oil inclusion; P_t: trapping pressure of oil inclusions; P_{hys}: hydrostatic pressure of the reservoir during oil cracking in an oil inclusion; P_{lis}: lithostatic pressure of the reservoir during oil cracking in an oil inclusion.

usually has a brown color under both transmitted and UV light (Bourdet et al., 2014).

Once oil is trapped in a fluid inclusion, it is very difficult for it to be altered to solid bitumen by gas deasphalting or biodegradation because oil inclusions are closed systems. Apart from oil cracking, the only possible mechanism that could produce solid bitumen after trapping of an oil inclusion is pressure reduction, which is often encountered during petroleum production, resulting in the plugging of the formation, wellbores and production facilities, and the isolation of oil from the flowing portion of the reservoir (Lichaa and Herrera, 1975). In addition, tectonic uplift can also result in pressure reduction in oil inclusions. However, these mechanisms are insignificant for the oil inclusions in this study, as most that have been examined do not contain solid bitumen.

Understanding the influence of oil cracking on T_{ho} has great geological significance in oil and gas exploration in deeply buried reservoirs. First, the modification by thermal stress of T_{ho} and P_t has been confirmed in this study. Researchers must be careful when reconstructing the oil charge history using oil inclusion data when the formation temperature is higher than 160 °C, especially when the oil inclusions experienced a maximum formation temperature of over 190 °C. Second, the uniform presence of black solid bitumen in oil inclusions is a valid factor for identifying whether the oil has been thermally cracked, and to determine the degree of oil cracking. The solid bitumen that is generated by oil cracking in a fluid inclusion assemblage should have the same volume ratio. The higher the F_{vpy} value, the higher the degree of oil cracking. If a single-phase liquid oil inclusion contains a large amount of solid bitumen with weak fluorescence or even no fluorescence, then the oil inclusion has experienced significant oil cracking, and oil and gas exploration should mainly focus on searching for gas that formed by secondary cracking of oil in ancient reservoirs.

Finally, overpressure will likely not develop according to the internal pressure changes in oil inclusions during oil cracking. Instead, hydrostatic pressure or underpressure (lower than the hydrostatic pressure) will develop during initial oil cracking in a closed system. Strong overpressure only develops during higher degrees of oil cracking. The absence of overpressure during initial oil cracking is beneficial for preserving in-situ oil cracked gas reservoirs, because strong overpressure from oil cracking will lower the gas/oil-water contact and release most of the oil and gas (Tian et al., 2008). Therefore, oil and gas exploration in deeply buried reservoirs should not ignore reservoirs with normal pressure or underpressure from lower-degree oil cracking, especially those with T_f between 150 °C and 190 °C, and focus on reservoirs with overpressure to ultra-high pressure with T_f higher than 190 °C.

5. Conclusions

(1) The beginning stages of oil cracking (T_r < 13%, T_f < 160 °C) have no obvious effect on the fluorescence color and intensity of oil inclusions. As the degree of oil cracking increases (T_r < 24%, T_f < 190 °C), oil inclusion fluorescence color shifts towards shorter wavelengths and the fluorescence

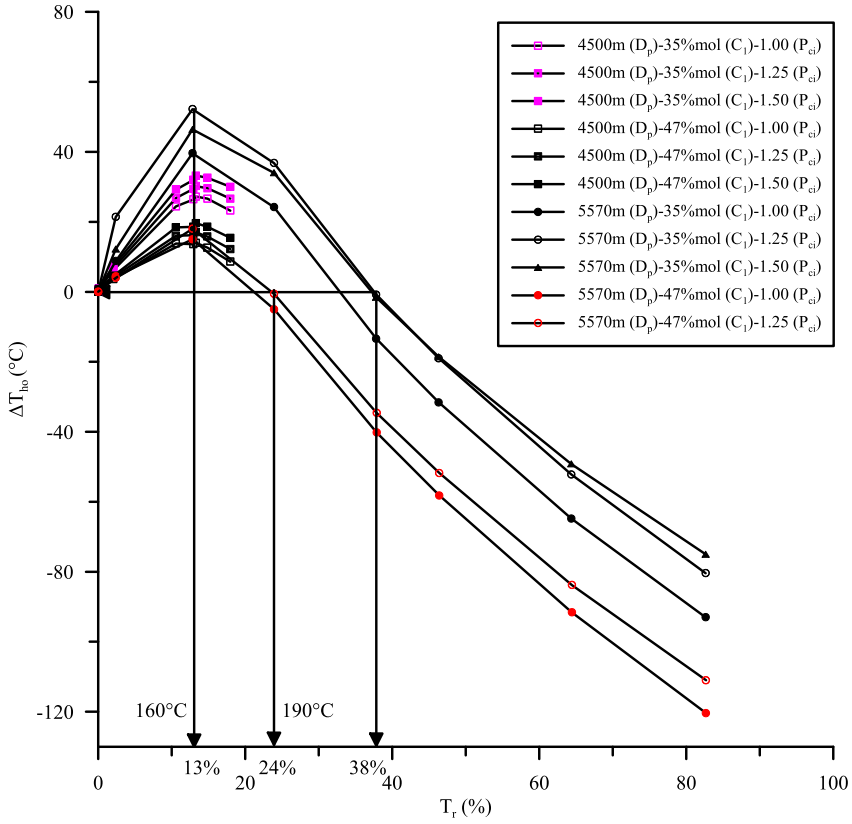

Fig. 16. The relationship between the transformation rate (T_r) during oil cracking and the homogenization temperature variation (ΔT_h) of oil inclusions during oil cracking. The present day burial depth (D_p) represents the thermal history that oil inclusions experienced after trapping, and C_1 represents the molar percent of methane in oil inclusions A and B.

intensity increases accordingly. As oil cracking progresses (T_r > 24%, T_f > 190 °C), the fluorescence color of an oil inclusion may not change obviously, or may continue to shift towards the blue color, accompanied by a decrease in fluorescence intensity. The fluorescence color will gradually change and even disappear as both the $C_{6\text{-}14}$ ARO and C_{14+} ARO components completely crack.

(2) The T_{ho} first increases and then decreases as oil cracking progresses. The inflection point appears at a temperature of approximately 160 °C, which corresponds to a T_r value of C_{6+} components of approximately 13%. When the T_r is higher than 13% and lower than 24% (160 °C < T_f < 190 °C), T_{ho} begins to decrease but is still larger than its initial homogenization temperature. T_{ho} becomes larger or smaller than its initial homogenization temperature depending on the initial trapping pressure value and the composition of the oil inclusion with a T_r value from 24% to 38%. T_{ho} becomes lower than its initial homogenization temperature once T_r is higher than 38%, and then T_{ho} continues to reduce until it reaches negative values, which corresponds to a single-phase liquid oil inclusion at room temperature. The reconstructed P_t has the opposite trend compared to T_{ho}, decreasing during the early stage of oil cracking (T_r < 13%) and then increasing.

(3) The degree of oil cracking in both oil inclusions and a reservoir can be estimated by the value of F_{vpy}, and then the modified extent of T_{ho} by oil cracking can be approximately predicted according to the relationship between ΔT_h and T_r. Investigating the distribution of pyrobitumen in oil inclusions should provide constraints on the depth and temperature conditions for oil cracking and thus the oil charge history reconstruction in deeply buried reservoirs.

(4) According to the variation in the internal pressure values of oil inclusions during oil cracking, a lower degree of crude oil cracking in reservoirs develops under normal pressure or underpressure rather than under overpressure conditions. Only under a higher degree of oil cracking (T_r > 40%) can overpressure and ultrahigh pressure be developed, possibly exceeding the lithostatic pressure (T_r > 70%).

(5) Oil inclusions from deeper than 4000 m in the DBRs in the Dongying Depression show consistent blue or blue-white fluorescence (λ_{max} < 500 nm), which was attributed to the oil cracking effect based on the general presence of solid bitumen in oil inclusions. The depth of 4000 m corresponds to a temperature of about 160 °C in the northern Dongying Depression, which is consistent with the modeling results. This suggests that a blue shift of fluorescence colors may occur in oil inclusions when the oil inclusions are heated above 160 °C.The relatively high T_{ho} of oil inclusions from deeper than 4000 m in the Minfeng area supports an increase in T_{ho} during low-degree oil cracking (T_f < 180 °C −190 °C, T_r < 24%). However, the effect of oil cracking on the T_{ho} may be unimportant when the oil inclusions were trapped under high overpressure.

(6) Oil cracking only results in hydrostatic pressure or underpressure during its early stages (T_r < 13–24%, T_f < 180–190 °C). Therefore, the exploration for oil and gas in deeply buried reservoirs cannot exclude the possibility of oil cracking to form gas reservoirs under conditions of underpressure or hydrostatic pressure, especially where the T_f ranges from 160 °C to 190 °C. Overpressure (T_r > 40%) that may even exceed lithostatic pressure (T_r > 70%) can occur with a high degree of oil cracking. Thus reservoirs with

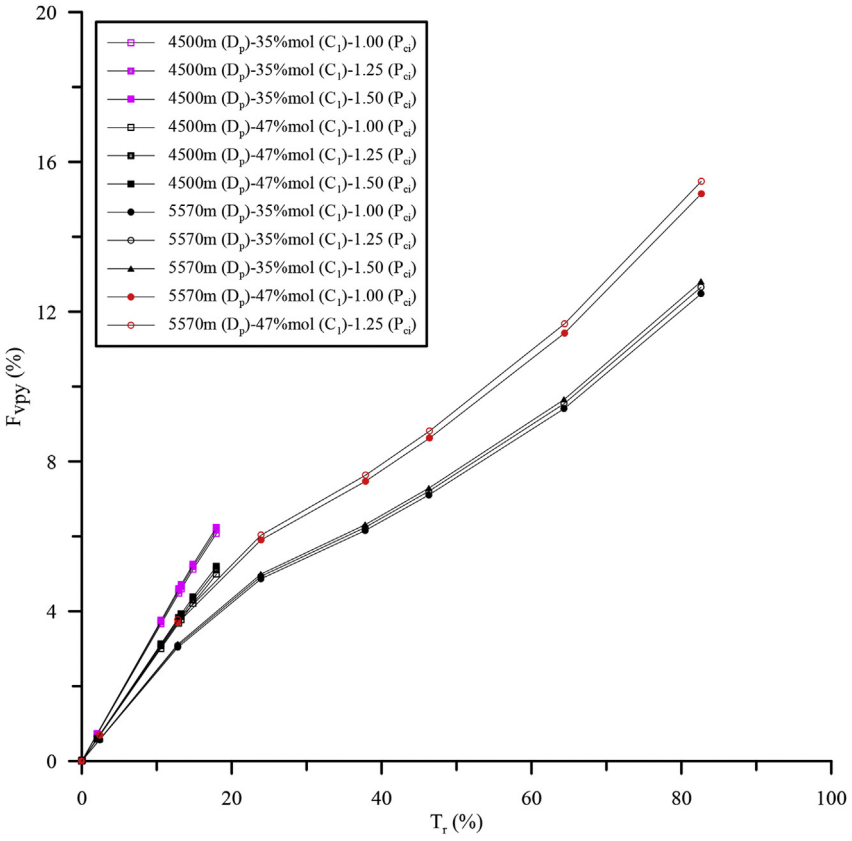

Fig. 17. The relationship between the transformation rate (T_r) during oil cracking and the volume percent of pyrobitumen (F_{vpy}). The present day burial depth (D_p) represents the thermal history that oil inclusions experienced after trapping, and C_1 represents the molar percent of methane in oil inclusions A and B.

overpressure or ultrahigh pressure, when the T_f is over 190 °C, could be potential exploration targets for oil cracked to gas in deep basins.

Acknowledgements

This work was supported by China's 973 National Key Research and Development Program (grant number 2012CB214804), the National Natural Science Foundation of China (NSFC) (grant number 41202088 and 41572118), and the Fundamental Research Funds for the Central Universities, China University of Geosciences (Wuhan) (grant number CUGL150408). The authors are indebted to Associated Editor Barry Jay Katz, and two anonymous reviewers for their careful and insightful comments and suggestions that have significantly improved the original manuscript. This paper was written whilst Dr. Hongwei Ping was a visiting scholar at the Department of Earth and Planetary Sciences, Macquarie University, the support of which is gratefully acknowledged.

Nomenclature

C_1	Methane
D	Depth (m)
D_p	Present-day burial depth (m)
D_t	Trapping depth of oil inclusion (m)
F_{vo}	Degree of bubble filling of oil inclusion (%)
F_{vpy}	Degree of pyrobitumen filling of oil inclusion (%)
P	Pressure (MPa)
P_{hys}	Hydrostatic pressure (MPa)
P_{lis}	Lithostatic pressure (MPa)
P_h	Homogenization pressure (saturation pressure) at homogenization temperature (MPa)
P_t	Trapping pressure (MPa)
P_v	Pressure at T_v (MPa)
T	Temperature (°C)
t	Time (Ma)
T_f	Formation temperature (°C)
T_r	Transformation rate of cracking of oil to gas (%)
T_h	Homogenization temperature (s) (°C)
T_{ho}	Homogenization temperature (s) of oil inclusion(s) (°C)
T_{ha}	Homogenization temperature (s) of aqueous fluid inclusion (s) (°C)
T_t	Trapping temperature (°C)
T_v	Measurement temperature of F_{vo} (°C)
ΔT_{ho}	The difference between the homogenization temperature of oil inclusion after oil cracking and initial homogenization temperature of oil inclusion trapped (°C)
ΔT_h	The difference between the T_{ha} of coeval aqueous fluid inclusions with oil inclusions and T_{ho} (°C)
ρ_{py}	Density of pyrobitumen (g/cm^3)
mol%	Molar percent
wt. %	Weight percent
CP	Critical point
L(G)	Bubble point line
G(L)	Dew point line
T_c	Critical temperature (K)
P_c	Critical pressure (MPa)
ω	Acentric factor
max	Maximum

Appendix A. Calculation of internal pressure of oil inclusion during oil cracking

It is assumed that the molar volume is V_m, the initial trapping pressure is P_{ti} and the mole number is m when an oil inclusion is trapped. The volume of liquid oil and insoluble solids (pyrobitumen and pyrobitumen predecessor) are V_{ot} and V_{st}, respectively, at time t, and the internal pressure during oil cracking is P_{ti}. At time t the mole number of crude oil is m_t, the molar volume is V_{mt}, and the quality and density of insoluble solids is M_{st} and ρ_{st}, respectively. Assuming that the volume of the oil inclusion does not change during oil cracking,

$$mV = V_{ot} + V_{st} \tag{A.1}$$

$$V_{ot} = m_t V_{mt} \tag{A.2}$$

$$V_{st} = M_{st}/\rho_{st} \tag{A.3}$$

In Eq. (A.1) to Eq. (A.3), m, m_t, M_{st} and ρ_{st} are controlled by the oil cracking kinetics and are all known quantities; V_{mt} is jointly controlled by the oil components, formation temperature and internal pressure of the oil inclusion. Therefore, an iterative calculation method can be applied to calculate the internal pressure changes of an oil inclusion during oil cracking. First, an initial internal pressure value of the oil inclusion is assigned and the liquid molar volume V_{mt} of the oil inclusion is calculated. If the calculated value does not match with Eq. (A.1), the initial value is changed until it satisfies the equation. Finally, the internal pressure after oil cracking can be obtained.

References

Al Darouich, T., Behar, F., Largeau, C., 2006. Pressure effect on the thermal cracking of the light aromatic fraction of Safaniya crude oil - implications for deep prospects. Org. Geochem 37, 1155–1169.

Allen, M.B., Macdonald, D.I.M., Xun, Z., Vincent, S.J., Brouet-Menzies, C., 1997. Early Cenozoic two-phase extension and late Cenozoic thermal subsidence and inversion of the Bohai Basin, northern China. Mar. Pet. Geol. 14, 951–972.

Aplin, A.C., Macleod, G., Larter, S.R., Pedersen, K.S., Sorensen, H., Booth, T., 1999. Combined use of Confocal Laser Scanning Microscopy and PVT simulation for estimating the composition and physical properties of petroleum in fluid inclusions. Mar. Pet. Geol. 16, 97–110.

Barker, C., 1990. Calculated volume and pressure changes during the thermal cracking of oil to gas in reservoirs. Am. Assoc. Pet. Geol. Bull. 74, 1254–1261.

Behar, F., Kressmann, S., Rudkiewicz, J.L., Vandenbroucke, M., 1992. Experimental simulation in a confined system and kinetic modelling of kerogen and oil cracking. Org. Geochem 19, 173–189.

Behar, F., Lorant, F., Mazeas, L., 2008. Elaboration of a new compositional kinetic schema for oil cracking. Org. Geochem 39, 764–782.

Bertrand, P., Pittion, J.-L., Bernaud, C., 1986. Fluorescence of sedimentary organic matter in relation to its chemical composition. Org. Geochem 10, 641–647.

Blanc, P., Connan, J., 1994. Preservation, degradation, and destruction of trapped oil. AAPG Mem. 60, 237.

Bloch, S., Lander, R.H., Bonnell, L., 2002. Anomalously high porosity and permeability in deeply buried sandstone reservoirs: origin and predictability. Am. Assoc. Pet. Geol. Bull. 86, 301–328.

Bourdet, J., Pironon, J., Levresse, G., Tritlla, J., 2008. Petroleum type determination through homogenization temperature and vapour volume fraction measurements in fluid inclusions. Geofluids 8, 46–59.

Bourdet, J., Pironon, J., Levresse, G., Tritlla, J., 2010. Petroleum accumulation and leakage in a deeply buried carbonate reservoir, Níspero field (Mexico). Mar. Pet. Geol. 27, 126–142.

Bourdet, J., Eadington, P., Volk, H., George, S.C., Pironon, J., Kempton, R., 2012. Chemical changes of fluid inclusion oil trapped during the evolution of an oil reservoir: Jabiru-1A case study (Timor Sea, Australia). Mar. Pet. Geol. 36, 118–139.

Bourdet, J., Burruss, R.C., Chou, I.M., Kempton, R., Liu, K.Y., Hung, N.V., 2014. Evidence for a palaeo-oil column and alteration of residual oil in a gas-condensate field: Integrated oil inclusion and experimental results. Geochim. Cosmochim. Ac 142, 362–385.

Burruss, R.C., 2003. Petroleum fluid inclusions, an introduction. In: Samson, Anderson, A., Marshall, D. (Eds.), Fluid Inclusions: Analysis and Interpretation. Mineral. Assoc. Can. Short Course Ser, pp. 159–174.

Cai, D., 2007. Research on the Pool-forming Mechanism of Pyrolysis Gas in the Medium-deep Zone of Lijin and Minfeng Area, Dongying Depression, Investigation and Exploration of Mineral Resource. China University of Petroleum, Dongying, p. 88 (in Chinese with English abstract).

Chang, C., 1991. Geological characteristics and distribution patterns of hydrocarbon deposits in the Bohai Bay Basin, east China. Mar. Pet. Geol. 8, 98–106.

Chen, Z., Ma, Z., Zha, M., Sha, X., Zhang, S., Bao, Y., 2014. The effect of high pressure on oil-to-gas cracking during laboratory simulation experiments. J. Pet. Geol. 37, 143–162.

Curiale, J.A., 1986. Origin of solid bitumens, with emphasis on biological marker results. Org. Geochem 10, 559–580.

Ding, F., Cai, J., Sui, F., Zheng, D., 2011. Characteristics of biomarker and Its implications of deeply buried source rocks from Northern Dongying Depression. Acta Sedimentol. Sin. 29, 192–198 (in Chinese with English abstract).

Dutkiewicz, A., Ridley, J., Buick, R., 2003. Oil-bearing CO_2-CH_4-H_2O fluid inclusions: oil survival since the Palaeoproterozoic after high temperature entrapment. Chem. Geol. 194, 51–79.

Evans, C.R., Rogers, M.A., Bailey, N.J.L., 1971. Evolution and alteration of petroleum in western Canada. Chem. Geol. 8, 147–170.

George, S.C., Ruble, T.E., Dutkiewicz, A., Eadington, P.J., 2001. Assessing the maturity of oil trapped in fluid inclusions using molecular geochemistry data and visually-determined fluorescence colours. Appl. Geochem 16, 451–473.

George, S.C., Ruble, T.E., Dutkiewicz, A., Eadington, P.J., 2002. Reply to comment by Oxtoby on Assessing the maturity of oil trapped in fluid inclusions using molecular geochemistry data and visually-determined fluorescence colours. Appl. Geochem 17, 1375–1378.

Giggenbach, W.F., 1997. Relative importance of thermodynamic and kinetic processes in governing the chemical and isotopic composition of carbon gases in high-heatflow sedimentary basins. Geochim. Cosmochim. Ac 61, 3763–3785.

Goldstein, R.H., 2001. Fluid inclusions in sedimentary and diagenetic systems. Lithos 55, 159–193.

Guilhaumou, N., Szydlowskii, N., Pradier, B., 1990. Characterization of hydrocarbon fluid inclusions by infra-red and fluorescence microspectrometry. Mineral. Mag. 54, 311–324.

Hanor, J.S., 1980. Dissolved methane in sedimentary brines; potential effect on the PVT properties of fluid inclusions. Econ. Geol. 75, 603–609.

Hantschel, T., Kauerauf, A.I., 2009. Fundamentals of Basin and Petroleum Systems Modeling. Springer.

Hao, F., Guo, T., Zhu, Y., Cai, X., Zou, H., Li, P., 2008. Evidence for multiple stages of oil cracking and thermochemical sulfate reduction in the Puguang gas field, Sichuan Basin, China. Am. Assoc. Pet. Geol. Bull. 92, 611–637.

Hill, R.J., Tang, Y., Kaplan, I.R., 2003. Insights into oil cracking based on laboratory experiments. Org. Geochem 34, 1651–1672.

Horsfield, B., McLimans, R.K., 1984. Geothermometery and geochemistry of aqueous and oil-bearing fluid inclusions from Fateh Field, Dubai. Org. Geochem 6, 733–740.

Horsfield, B., Schenk, H.J., Mills, N., Welte, D.H., 1992. An investigation of the in-reservoir conversion of oil to gas: compositional and kinetic findings from closed-system programmed-temperature pyrolysis. Org. Geochem 19, 191–204.

Hu, A., Li, M., Wong, J., Reyes, J., Achal, S., Milovic, M., Robinson, R., Shou, J., Yang, C., Dai, J., Ma, Y., Guo, T., 2010. Chemical and petrographic evidence for thermal cracking and thermochemical sulfate reduction of paleo-oil accumulations in NE Sichuan Basin, China. Org. Geochem 41, 924–929.

Huang, W.-L., Otten, G.A., 2001. Cracking kinetics of crude oil and alkanes determined by diamond anvil cell-fluorescence spectroscopy pyrolysis: technique development and preliminary results. Org. Geochem 32, 817–830.

Hui, Tian, Zhaoming, Wang, Zhongyao, Xiao, Xianqing, Li, Xianming, Xiao, 2006. Oil cracking to gases: kinetic modeling and geological significance. Chin. Sci. Bull. 51, 2763–2770.

Hunt, J.M., 1995. In: Freeman, W.H. (Ed.), Petroleum Geochemistry and Geology, second ed.

Isaksen, G.H., 2004. Central North Sea hydrocarbon systems: generation, migration, entrapment, and thermal degradation of oil and gas. Am. Assoc. Pet. Geol. Bull. 88, 1545–1572.

Jacob, H., 1989. Classification, structure, genesis and practical importance of natural solid oil bitumen ("migrabitumen"). Int. J. Coal Geol. 11, 65–79.

Karlsen, D.A., Nedkvitne, T., Larter, S.R., Bjørlykke, K., 1993. Hydrocarbon composition of authigenic inclusions: application to elucidation of petroleum reservoir filling history. Geochim. Cosmochim. Ac 57, 3641–3659.

Khorasani, G.K., 1987. Novel development in fluorescence microscopy of complex organic mixtures: application in petroleum geochemistry. Org. Geochem 11, 157–168.

Kuo, L.-C., Michael, G.E., 1994. A multicomponent oil-cracking kinetics model for modeling preservation and composition of reservoired oils. Org. Geochem 21, 911–925.

Li, P.-L., 2004. Oil/gas distribution patterns in Dongying depression, Bohai Bay Basin. J. Pet. Sci. Eng. 41, 57–66.

Lichaa, P.M., Herrera, L., 1975. Electrical and other effects related to the formation and prevention of asphaltene deposition problem in Venezuelan crudes. In: SPE Oilfield Chemistry Symposium. Society of Petroleum Engineers, SPE-5304-MS, Dallas, Texas.

McLimans, R.K., 1987. The application of fluid inclusions to migration of oil and diagenesis in petroleum reservoirs. Appl. Geochem 2, 585–603.

McNeil, R.I., BeMent, W.O., 1996. Thermal stability of hydrocarbons: laboratory criteria and field examples. Energy & Fuels 10, 60–67.

Munz, I.A., 2001. Petroleum inclusions in sedimentary basins: systematics,

analytical methods and applications. Lithos 55, 195–212.
Munz, I.A., Wangen, M., Girard, J.-P., Lacharpagne, J.-C., Johansen, H., 2004. Pressure-temperature-time-composition (P-T-t-X) constraints of multiple petroleum charges in the Hild field, Norwegian North Sea. Mar. Pet. Geol. 21, 1043–1060.
Okubo, S., 2005. Effects of thermal cracking of hydrocarbons on the homogenization temperature of fluid inclusions from the Niigata oil and gas fields, Japan. Appl. Geochem 20, 255–260.
Oxtoby, N.H., 2002. Comments on: assessing the maturity of oil trapped in fluid inclusions using molecular geochemistry data and visually-determined fluorescence colours. Appl. Geochem 17, 1371–1374.
Pang, X., Li, M., Li, S., Jin, Z., 2003. Geochemistry of petroleum systems in the Niuzhuang South Slope of Bohai Bay Basin. Part 2: evidence for significant contribution of mature source rocks to “immature oils” in the Bamianhe field. Org. Geochem 34, 931–950.
Peng, D., Robinson, D., 1976. A new two-constant equation of state. Ind. Eng. Chem. Fundam. 15, 59–64.
Ping, H., Chen, H., 2011. Main controlling factors on oil inclusion homogenization temperatures and their geological significance. Earth Sci – J China Univ. Geosci. 36, 131–138 (in Chinese with English abstract).
Ping, H., Thiéry, R., Chen, H., 2011. Thermodynamic modelling of petroleum inclusions: the prediction of the saturation pressure of crude oils. Geofluids 11, 328–340.
Ping, H., Chen, H., Song, G., Liu, H., 2012. Individual oil inclusion composition prediction and its application in oil and gas accumulation studies. Earth Sci – J China Univ. Geosci. 37, 815–824 (in Chinese with English abstract).
Ping, H., Chen, H., Thiéry, R., 2013. Thermodynamic modeling of petroleum inclusions: composition modeling and prediction of the trapping pressure of crude oils. Fluid Phase Equilib. 346, 33–44.
Ping, H., Chen, H., Jia, G., 2017. Petroleum accumulation in the deeply buried reservoirs in the northern Dongying Depression, Bohai Bay Basin, China: new insights from fluid inclusions, natural gas geochemistry, and 1-D basin modeling. Mar. Pet. Geol. 80, 70–93.
Pironon, J., Bourdet, J., 2008. Petroleum and aqueous inclusions from deeply buried reservoirs: experimental simulations and consequences for overpressure estimates. Geochim. Cosmochim. Ac 72, 4916–4928.
Pironon, J., Pradier, B., 1992. Ultraviolet-fluorescence alteration of hydrocarbon fluid inclusions. Org. Geochem 18, 501–509.
Price, L.C., 1993. Thermal stability of hydrocarbons in nature: limits, evidence, characteristics, and possible controls. Geochim. Cosmochim. Ac 57, 3261–3280.
Riecker, R.E., 1962. Hydrocarbon fluorescence and migration of petroleum. Am. Assoc. Pet. Geol. Bull. 46, 60–75.
Roedder, E., 1984. Fluid Inclusions. Mineralogical Society of America, Washington.
Snape, C.E., Meredith, W., Uguna, C., Car, A.D., 2007. Retaration of oil cracking in high-pressure liquid water. Abstr. Rep. - Int. Congr. Org. Geochem. 23, 35–36.
Teinturier, S., Elie, M., Pironon, J., 2003. Oil-cracking processes evidence from synthetic petroleum inclusions. J. Geochem Explor 78–79, 421–425.
Thiéry, R., 2006. Thermodynamic modelling of aqueous CH_4-bearing fluid inclusions trapped in hydrocarbon-rich environments. Chem. Geol. 227, 154–164.
Thiéry, R., Pironon, J., Walgenwitz, F., Montel, F., 2002. Individual characterization of petroleum fluid inclusions (composition and P-T trapping conditions) by microthermometry and confocal laser scanning microscopy: inferences from applied thermodynamics of oils. Mar. Pet. Geol. 19, 847–859.
Tian, H., Xiao, X., Wilkins, R.W.T., Tang, Y., 2008. New insights into the volume and pressure changes during the thermal cracking of oil to gas in reservoirs: Implications for the in-situ accumulation of gas cracked from oils. Am. Assoc. Pet. Geol. Bull. 92, 181–200.
Tissot, B., Espitalié, J., 1975. L'evolution thermique de la matière organique des sédiments : applications d'une simulation mathématique. Potentiel pétrolier des bassins sédimentaires de reconstitution de l'histoire thermique des sédiments. Oil Gas. Sci. Technol. - Rev. IFP 30, 743–778.
Tissot, B.P., Welte, D.H., 1984. Petroleum Formation and Occurrence. Springer-Verlag, New York.
Tseng, H.-Y., Pottorf, R.J., 2002. Fluid inclusion constraints on petroleum PVT and compositional history of the Greater Alwyn–South Brent petroleum system, northern North sea. Mar. Pet. Geol. 19, 797–809.
Tsuzuki, N., Takeda, N., Suzuki, M., Yokoi, K., 1999. The kinetic modeling of oil cracking by hydrothermal pyrolysis experiments. Int. J. Coal Geol. 39, 227–250.
Ungerer, P., Behar, F., Villalba, M., Heum, O.R., Audibert, A., 1988. Kinetic modelling of oil cracking. Org. Geochem 13, 857–868.
Vandenbroucke, M., Behar, F., Rudkiewicz, J.L., 1999. Kinetic modelling of petroleum formation and cracking: implications from the high pressure/high temperature Elgin Field (UK, North Sea). Org. Geochem 30, 1105–1125.
Wang, R., 2009. Geochemical characteristics and source of light oil in the deep Es4L layers underlying salt in the northern Dongying Depression. Nat. Gas. Geosci. 20, 278–281 (in Chinese with English abstract).
Wilkinson, M., Haszeldine, R.S., 2011. Oil charge preserves exceptional porosity in deeply buried, overpressured, sandstones: central North Sea, UK. J. Geol. Soc. 168, 1285–1295.
Yang, X., Sui, F., Li, W., Wang, W., 2007. The main controlling factors of cracked gas accumulation in deeply buried reservoirs in Dongying Depression. Xinjiang Pet. Geol. 28, 563–565 (in Chinese with English abstract).
Yong, Z., 2006. The Structure, Strata Sequence and Oil Pool Forming Dynamics in the Northern Slope in the Dongying Depression. Petroleum Industry Press, Beijing (in Chinese).
Zhao, W., Zhang, S., Wang, F., Chen, J., Xiao, Z., Song, F., 2005. Gas accumulation from oil cracking in the eastern Tarim Basin: a case study of the YN2 gas field. Org. Geochem 36, 1602–1616.